Venous-derived angioblasts generate organ-specific vessels during embryonic development

Authors:

Gideon Hen[1,4], Julian Nicenboim[1,4], Oded Mayseless[1], Lihee Asaf[1], Masahiro Shin[2], Giorgia Busolin[3], Roy Hofi[1], Gabriella Almog[1], Natascia Tiso[3], Nathan D. Lawson[2] and Karina Yaniv[1*]

Affiliations:

1. Department of Biological Regulation, Weizmann Institute of Science, Rehovot 76100, Israel.

2. Program in Gene Function and Expression, University of Massachusetts Medical School, Worcester, MA 01605 USA.

3. Department of Biology, University of Padova, Padova I-35131, Italy

4. These authors contributed equally to this work

* Corresponding author:

Karina Yaniv

Department of Biological Regulation

Weizmann Institute of Science

Rehovot, 76100 Israel

Email: karina.yaniv@weizmann.ac.il

Tel.: 972-8-9342224

Fax: 972-8-9344186

Development • Advance article

ABSTRACT

Formation and remodeling of vascular beds are complex processes orchestrated by multiple signaling pathways. While it is well accepted that vessels of a particular organ display specific features that enable them to fulfill distinct functions, the embryonic origins of tissue-specific vessels, as well as the molecular mechanisms regulating their formation, are poorly understood. The subintestinal plexus of the zebrafish embryo comprises vessels that vascularize the gut, liver and pancreas, and as such represents an ideal model to investigate the early steps of organ-specific vessel formation. Here we show that both arterial and venous components of the subintestinal plexus originate from a pool of specialized angioblasts residing in the floor of the Posterior Cardinal Vein (PCV). Using live imaging of zebrafish embryos, in combination with photoconvertable transgenic reporters, we demonstrate that these angioblasts undergo two phases of migration and differentiation. Initially, a subintestinal vein (SIV) forms and expands ventrally through a bone morphogenetic protein (BMP)-dependent step of collective migration. Concomitantly, a VEGF-dependent shift in the directionality of migration, coupled to the upregulation of arterial markers is observed, which culminates with the generation of the supraintestinal artery (SIA). Altogether our results establish the zebrafish subintestinal plexus as an advantageous model for the study of organ-specific vessel development, and provide new insights into the molecular mechanisms controlling its formation. More broadly, our findings suggest that PCV-specialized angioblasts contribute not only to the formation of the early trunk vasculature, but also to the establishment of late forming-, tissue specific vascular beds.

INTRODUCTION

Establishment of a functional vascular system is essential for proper tissue development. In vertebrates, this process involves the formation of the main axial vessels through vasculogenesis, followed by a step of sprouting angiogenesis, to generate the systemic vasculature (Adams and Alitalo, 2007). Later on, as development proceeds, additional vascular beds form in order to support the establishment, growth and proper functionality of different organs. At present it is well accepted that vessels of a particular organ display specific features that enable them to fulfill distinct functions (Cleaver, 2004; Aird, 2007). While a large bulk of data describing the development of the systemic vasculature has accumulated during the past decades (Potente et al., 2011), little is known about the embryonic origins and the molecular mechanisms underlying the formation of organ-specific vessels (Nolan et al., 2013).

Formation of the gastrointestinal (GI) tissues was shown to follow the establishment of the cardiovascular system. Therefore, organs develop in the presence of already formed blood vessels and adjacent endothelial cells (ECs) (Lammert et al., 2003; Nikolova and Lammert, 2003). Signals derived from the endothelium are thought to establish the location, differentiation and morphology of the gastrointestinal organs. In turn, these organs drive adjacent ECs to acquire unique features in order to meet their specific needs (Nikolova and Lammert, 2003). That is the case for instance, of liver sinusoidal ECs (LSECs), which possess fenestrae that can modify their size in response to different agents (Braet et al., 1995), or of beta cells in pancreatic islets that are thought to secrete insulin into the blood stream, through endothelial fenestrae (Nikolova and Lammert, 2003), These examples clearly demonstrate the need for mutual feedback and interaction between the tissues and their surrounding endothelium, in order to generate a specific functional vasculature.

Previous reports analyzing the development of the zebrafish GI tract have described the intimate interaction between the organs and the vasculature in this system. At 24 hpf, endoderm-derived cells form the intestinal rod in the zebrafish midline (Field et al., 2003a). By 52 hpf the alimentary canal, including the pharynx, oesophagus, intestinal bulb and posterior intestine, is fully discernible (Field et al., 2003a; Wallace and Pack, 2003), and is entirely wrapped by the subintestinal vein (SIV), supraintestinal artery (SIA) and interconnecting vessels (ICVs) at 5.5-7.5 dpf (Isogai et al., 2001). In the case of the liver, vascularization is thought to begin at 36 hpf when the first ECs are found adjacent to the liver bud (Field et al., 2003a). By ~60 hpf hepatic vessels have reached and penetrated the hepatocyte surfaces, populating the entire liver by 72 hpf (Korzh et al., 2008). In the mouse, liver development begins at E8.5-9, when cells from the endoderm give rise to the liver bud.

Half a day later, ECs surround the liver endoderm and intermingle with delaminating liver cells (Matsumoto et al., 2001). In rat, the definitive structural differentiation of LSECs was suggested to be achieved only in the perinatal period (Barbera-Guillem et al., 1986). Mature LSECs display the characteristic structure of unique capillaries showing open pores or fenestrae, and lacking a diaphragm and a basal lamina underneath the endothelium (Braet and Wisse, 2002). The role of ECs in liver development is still under debate. In mouse embryos, for instance, ECs were shown to be necessary for hepatic formation (Matsumoto et al., 2001). In zebrafish the results have remained controversial, with some reports showing that initial liver development takes place normally in embryos lacking a well-developed vasculature (Field et al., 2003a), wile others claim that ECs are essential for polarization of hepatocytes and proper liver formation (Sakaguchi et al., 2008), as well as during late stages of liver morphogenesis (Korzh et al., 2008). Most recently, LSECs were shown to enhance hepatic regeneration and repair in the mouse, through the release of angiocrine factors (Ding et al., 2010; Ding et al., 2014; Hu et al., 2014), highlighting the important clinical implications of tissue-specific vascular beds.

The development of the pancreas has been extensively studied both in mouse and zebrafish (Edlund, 2002; Murtaugh, 2007). In mouse embryos, ventral and dorsal pancreatic buds develop from the endoderm at E8.5–E9.5, and give rise to both endocrine and exocrine cells (Kim and Hebrok, 2001; Lammert et al., 2001). In the zebrafish, in contrast, the dorsal posterior bud gives rise only to endocrine cells, whereas the ventral anterior bud generates both exocrine and endocrine cells (Field et al., 2003b). The zebrafish pancreas was shown to form via fusion of a posterior and anterior pancreatic buds at around 52 hpf (Field et al., 2003b). While the posterior pancreatic bud lies in contact with the main axial vessels at already 24 hpf, only by ~52 hpf the first ECs are detected throughout the developing pancreas (Field et al., 2003b). ECs were shown to be necessary for the formation of the pancreas in mouse and *Xenopus* (Lammert et al., 2001). Endothelium of the aorta for instance, was shown to induce budding of the dorsal pancreatic endoderm, thereby promoting endocrine development (Lammert et al., 2001). In similar fashion, only the ventral pancreatic bud adjacent to the endothelium of the right vitelline vein develops into pancreatic tissue, whereas the other bud regresses (Lammert et al., 2001). The central role of the endothelium in pancreatic development was further supported by findings demonstrating that EC-endoderm interactions are essential for expression of PDX1 and insulin in isolated mouse embryonic tissues (Lammert et al., 2001), and promote dorsal pancreatic development via Ptf1a, which is required for pancreatic lineage specification (Yoshitomi and Zaret, 2004). While these studies, point to a clear role for the endothelium during pancreatic development, early

morphogenesis and differentiation of the zebrafish pancreas appear normal in embryos devoid of endothelial cells (Field et al., 2003b).

The subintestinal plexus of the developing zebrafish embryo comprises vessels that vascularize the gut, liver and pancreas, and as such represents an ideal model to investigate the early steps of organ-specific vessel formation. This vascular bed develops on both sides of the yolk ball (Isogai et al., 2001) and includes the SIA, SIV and ICVs. In contrast to the intersegmental vessels (ISVs) of the trunk, which sprout following well-defined attracting and repulsive cues (Torres-Vazquez et al., 2004; Suli et al., 2006), the subintestinal plexus develops in the absence of any apparent tissue guiding its formation. Yet, these vessels generate a highly stereotypical basket-shaped structure, which acquires its mature form at approximately 3 dpf (Isogai et al., 2001; Lenard et al., 2015).. Although established as a model for the study of metabolic regulation of angiogenesis (Avraham-Davidi et al., 2012), drug evaluation (Serbedzija et al., 1999) and for assaying tumor angiogenesis (Nicoli and Presta, 2007), very little is known about the embryonic origins and molecular mechanisms regulating formation of the subintestinal plexus. The first anatomical description of the subintestinal plexus and its derivatives, was obtained through the use of confocal micro-angiography (Isogai et al., 2001). Most recently, a report by Lenard et al. (Lenard et al., 2015) provided the first characterization of the morphological events underlying the formation of the subintestinal plexus, and established it as a powerful model for the study of vessel pruning.

Here, we investigate the different steps underlying the embryonic development of the subintestinal plexus, and provide a thorough characterization of its interactions with the nascent digestive system. We find that in contrast to previously proposed models claiming contribution of the DA to the formation of organ specific vessels, both the arterial and venous components of the zebrafish subintestinal plexus share a venous origin. We further use live imaging of transgenic zebrafish, in combination with lineage tracing approaches, to characterize the sequence of events involved in shaping the subintestinal plexus, and identify the molecular cues controlling each step. Altogether, our findings provide new insights into the origins and development of the gastrointestinal vasculature in the zebrafish embryo, establishing it as an advantageous model for the study of organ specific vessel development.

RESULTS

Anatomical and molecular characterization of the subintestinal plexus

Previous reports have provided a clear anatomical characterization of the subintestinal plexus in zebrafish and medaka (Isogai et al., 2001; Fujita et al., 2006), and have defined the identity of the different vessels comprising this network, based on confocal microangiography analyses. Confocal imaging of 3.5 dpf *Tg(fli1:EGFP^{y1};gata1a:dsRed^{sd2})* (Yaniv et al., 2006) embryos revealed the presence of rostro-caudal blood flow in the SIA, whereas circulation in the SIV followed the directionality observed in the PCV (Fig. 1A, white arrows). Interestingly, we observed uniform dorso-ventral flow (from the SIA to the SIV) in all of the ICVs (Fig. 1A, white arrows). In order to ascertain whether this functional characterization is supported by distinct expression of well-established arterial-venous markers, we imaged transgenic zebrafish embryos at 4-5 dpf. As seen in Fig. 1B, clear expression of the lymph-venous marker *lyve1* was detected in the PCV, thoracic duct (TD), SIV and ICVs, but not in the dorsal aorta (DA) and SIA of *Tg(fli1:EGFP;lyve1:dsRed2^{nz101})* (Nicenboim et al., 2015) double transgenic embryos, indicating the venous identity of these vessels. In contrast, in the arterial specific *Tg(flt1_9a_cFos:GFP)^{wz2}* reporter (Nicenboim et al., 2015) only the DA and SIA displayed strong GFP fluorescence (Fig. 1C), indicating that aside of the SIA, all components of the subintestinal plexus share a venous identity.

Origin of the subintestinal vessels

One of the major questions regarding the development of organ-specific vascular networks has to do with their embryonic origins. Since the subintestinal plexus has been regarded as one of the possible origins of the GI tract vasculature, we decided to investigate the relative contribution of surrounding vessels to its formation, using photoconversion of ECs (Fig. 2 and Fig. S1). We began by photoswitching all ECs in the DA of *Tg(fli1:gal4^{ubs3};uas:kaede^{rk8})* (Herwig et al., 2011) embryos at 1 dpf. Surprisingly, no red/photoconverted cells were detected in the subintestinal plexus at 2.5 dpf (Fig. 2A), suggesting that arterial-derived ECs do not contribute to the formation of this vascular bed. We have recently uncovered the presence of specialized angioblasts within the ventral PCV (vPCV), which generate arterial, venous and lymphatic ECs (Nicenboim et al., 2015). We thus wondered whether these angioblasts serve as a source for late-forming vessels, such as the subintestinal plexus. Photoconversion of vPCV cells rendered red fluorescent cells in all vessels of the subintestinal plexus including the SIA (Fig. 2C, arrowheads), indicating the venous origin of all components of the digestive system's vasculature. This was in contrast to cells of the

dorsal PCV (dPCV) that following photoswitching were found only in the intersegmental vessels of the trunk (Fig. 2B, and data not shown). Interestingly, we noticed that the most rostral part of the SIV was not populated by red-labeled vPCV cells or by their progeny (Fig. 2C). To identify the origin of these cells we photoconverted the left branch of the anterior portion of the PCV (aPCV), which also represents the SIV drainage point. As seen in Fig. 2D, red ECs were found in the rostral most part of the SIV in all analyzed embryos, indicating that the aPCV is not only connected to the SIV, but also contributes to its formation. Finally, no red cells were detected in the subintestinal plexus of 2.5 dpf embryos following photoconversion of the common cardinal vein (CCV) at 24 hpf (Fig. 2E), highlighting the vPCV angioblasts as the major source of ECs generating the subintestinal plexus.

The subintestinal plexus gives rise to the digestive system's vasculature

In order to analyze the anatomical distribution of the subintestinal vessels with respect to the different organs of the digestive system, we first mated *Tg(fli1:dsRed)*^{um13} (Covassin et al., 2009) and *Tg(gut:GFP)*^{s854} (Field et al., 2003a) fish, in which GFP labels the endoderm and its derivatives. The spatio-temporal interaction of the plexus and the liver was examined by confocal microscopy between 36 hpf - 4 dpf (Fig. 3 and Fig. S2). At 36 hpf the left branch of the aPCV is detected in close proximity to the developing liver (Fig. 3A, "L"), which appears later on (54 hpf) wrapped by both the aPCV and the most rostral part of the SIV (Fig. 3B), and (Isogai et al., 2001; Ober et al., 2003). At 72 hpf the liver hepatic vessels (HV) are fully established by ECs arising in the left aPCV and the anterior part of the left SIV, which drains into the liver as the hepatic portal vein (HPV) (Fig. 3C). Towards 4 dpf the hepatic vessels have acquired their typical reticular anatomy (Fig. S2A-A''). The contribution of the subintestinal plexus to the HVs was further addressed using *Tg(fli1:gal4*^{ubs3}*;uas:kaede*^{rk8}*)* embryos. Photoconversion of the left branch of the aPCV at 29 hpf resulted in red cells populating the liver 24 hrs later (Fig. 3D, 55 hpf, white arrowheads). Likewise, photoconversion of the left SIV at 48 hpf rendered red cells that populated the HVs by 72 hpf (Fig. 3E, white arrowheads). Together, these results demonstrate that both the left aPCV, and the rostral part of the SIV, contribute to the liver vasculature, and confirm that at these early stages of development, the hepatic vessels originate from the PCV or its derivatives, with no apparent arterial contribution.

The vasculature of the intestinal bulb (IB) was similarly examined (Fig. S3). At 36 hpf the first ECs leave the floor of the PCV and sprout ventrally right on top of the intestinal bulb (Fig. S3A). Between 36 - 52 hpf the intestine undergoes extensive morphogenesis and growth (Ng et al., 2005) (Fig. S3A,B), until it acquires its final position on the left side at

approximately 72 hpf (Fig. S3C). Throughout this entire process the IB is engulfed by the ICVs of the subintestinal plexus (Fig. S3B,C and Movie 1), and is entirely wrapped by the SIV, SIA and ICVs at later stages (Fig. S2B, S3C and Movie 1) and (Isogai et al., 2001). To study the pancreas vasculature, *Tg(fli1:dsRed)*^{um13} were mated with *Tg(-1.0ins:EGFP)*^{sc1} (diIorio et al., 2002) fish, in which cells of the endocrine pancreas are highlighted in green (Fig. 4 and Fig. S2C). Confocal imaging of double transgenic embryos confirmed the gradual shift of the pancreatic anlage from a medial position at 36 hpf towards the right side of the midline (Field et al., 2003b), beneath the right aPCV (Fig. 4A-C). By 62 hpf the pancreatic anlage is positioned between the right SIV and the right aPCV; the most cranial ICV on the right side of the plexus, interconnects the SIV and the SIA to form the pancreatic vessels (Fig. 4C, arrowhead and Fig. S2C). Photoconversion of either the right aPCV at 29 hpf, or the most rostral part of the SIV at 48 hpf resulted in red labeling of the pancreatic vasculature at 55 and 72 hpf, respectively (Fig. 4D,E, arrowheads). In addition, the direct contribution of ECs from the aPCV and SIV to the pancreatic vasculature was tracked *in vivo.* Following focused photoswitching on *Tg(fli1:gal4;uas:kaede;-1.0ins:EGFP*) embryos, time-lapse confocal microscopy was used in order to follow the generation of the pancreatic vasculature from the aPCV and SIV between 54-73.5 hpf (Movie 2). Taken together these data indicate that the vasculature of at least three different organs of the digestive system originates in the PCV, either directly, or through the intermediate subintestinal plexus. Furthermore these findings highlight the plasticity of the vPCV angioblasts and their ability to contribute to different vessel types.

Different mechanisms of EC migration underlie the formation of the subintestinal plexus

In order to investigate the dynamics of formation of the subintestinal plexus, we live-imaged *Tg(fli1:dsRed*^{um13}*;fli1:nGFP*^{y17}*)* double transgenic embryos in time lapse, between 30-90 hpf (Fig. 5A,C and Movie 1). At 32 hpf we detected short ventral sprouts arising from the vPCV, which quickly anastomose to generate a single vessel (Fig. 5A, 32,35 hpf, white arrowheads) that extends rostrally and fuses with a caudal projection arising from the aPCV (Fig. 5A, 32,35 hpf, red arrowhead). This newly formed primary SIV undergoes extensive remodeling involving the fusion of angiogenic sprouts (Fig. 5A, 35-41 hpf, white arrowheads), and formation of vascular loops (Fig. 5A, green asterisks), until the establishment of a mature SIV is achieved, The ventral migration of the mature SIV is then guided by 3 to 5 short "leading buds" (Fig. 5A, 56 hpf, arrows), which later on retract, rendering the stereotypical subintestinal basket shape by ~70-80 hpf (Fig. 5A,C, and Movie 1). During these last steps active pruning of the cross branches is also observed (Lenard et al., 2015). Along with the ventral expansion of the plexus, we detected ECs migrating dorsally from the SIV to populate the SIA (Fig. 5A, 39-41 hpf, light-blue arrowheads and Fig. 5C). In

order to ascertain whether the same vPCV cells that populate the SIV also incorporate into the SIA, we tracked the migration of individual ECs in *Tg(fli1:dsRed;fli1:nGFP)* embryos between 30-60 hpf (Fig. 5B,C and Movie 3). We found that vPCV angioblasts (Fig. 5B, 34.75 hpf, and Fig. 5C) leave the PCV at ~36 hpf and migrate ventrally to incorporate into the primary SIV (Fig. 5B, 36-51.5 hpf, and Fig. 5C). Some of these cells will then engage in dorsal migration to end up populating the SIA (Fig. 5B, 55.25 to 59.75 hpf, blue arrowhead, and Fig. 5C). Altogether, our time-lapse analyses reveal that vPCV angioblasts contribute to all components of the subintestinal plexus through two different phases of migration: initially they sprout from the PCV, anastomose, and migrate ventrally to generate a mature SIV. While the ventral expansion of the SIV and ICVs takes place, some cells lag back shortly and migrate dorsally to generate the arterial component of the plexus (Fig. 5C and Movie 3, blue arrow)

During active angiogenesis, formation and growth of new sprouts involve coordination between opposing tip and stalk cell behaviors, a process that is tightly regulated by the VEGF and Notch signaling pathways (Hellstrom et al., 2007; Siekmann and Lawson, 2007; Jakobsson et al., 2010). Interestingly however, our live-imaging analyses revealed a step of collective migration involved in formation of the subintestinal plexus, whereby the SIV extends ventrally as a single unit, and not through the classic tip/stalk- cell mechanism. By following actin dynamics in ECs using *Tg(fli1:lifeact-GFP)*^{wz4} embryos (Fig. 6A-C), we detected the presence of numerous actin-rich filopodia in the leading buds at the migration front (Helker et al., 2013) (Fig 6B, arrows), a behavior similar to that observed in ISV tip cells (Phng et al., 2013), and in the vascular front of the postnatal mouse retina (Gerhardt et al., 2003). These features were apparent throughout the entire phase of formation of the mature SIV and its subsequent ventral expansion, but were no longer evident as ventral migration ceased by 3 dpf (Fig. 6C). Examination of the spatial distribution of the EC-nuclei in the SIV of *Tg(fli1:nGFP)* embryos (Fig. 6D and Movie 4) revealed that ~80% of the leading buds consisted of paired ECs positioned in parallel to each other, rather than of a single tip cell (Fig. 6D, 48-55 hpf, arrowheads). Moreover, none of these nuclei exhibited dominancy over its neighbor, and both remained adjacent to each other throughout the entire phase of ventral migration. As ventral expansion of the plexus approached termination, ECs constituting each of the leading buds incorporated into the SIV or migrated dorsally to populate the ICVs (Fig. 6D, 69 hpf, arrowheads, and Movie 4).

Given the importance of Notch signaling in coordinating vessel sprouting in other contexts, we assessed the role of this pathway during formation of the subintestinal plexus. We began by analyzing the effects of the γ-Secretase inhibitor DAPT following treatment of *Tg(fli1:dsRed;flt1_9a_cFos:GFP)* embryos between 24-72 hpf (Fig. 7). Unlike DMSO-

treated control siblings, in which the stereotypical basket shape has been consolidated by 3 dpf (Fig. 7A), in embryos raised in the presence of 100μM DAPT the retraction of the leading buds during the final stages of SIV remodeling was inhibited (Fig. 7A-D). In addition, we detected defects in formation of the SIA, including marked reduction in the expression of the arterial marker *flt1_9a_cFos:GFP* (Fig. 7B, asterisks), suggesting that Notch signaling is required for proper formation of a functional SIA including its arterial differentiation. In addition to the impaired retraction of leading buds induced by DAPT treatment, we also detected persistent filopodia along the entire SIV by 72 hpf (Fig. 7C, arrows). These findings are in line with previous reports describing excessive filopodia formation following DAPT treatment in the ISVs of the zebrafish trunk (Leslie et al., 2007). To further corroborate these results, we examined the pattern of Notch activation in the subintestinal plexus using the *Tg(EPV.Tp1-Mmu.Hbb:EGFP)*^{ia12} (12xNRE:EGFP) reporter line (Fig. S4). This reporter, which consists of 12 repeats of Notch-responsive elements driving EGFP expression (Moro et al., 2013), is specifically responsive to Notch signaling, as manifested by its dose-dependent down-regulation in response to DAPT treatment (Fig. S4). Analysis of transgenic embryos between 35 - 60 hpf revealed Notch activation in the DA and arterial ISVs (Fig. 7E, and data not shown) (Quillien et al., 2014).Yet, no Notch-derived fluorescence was observed in the subintestinal plexus until ~ 50 to 60 hpf, where Notch positive cells were detected in the SIA (Fig. 7E, 50, 60 hpf, arrowheads) (Lawson et al., 2001; Lawson and Weinstein, 2002; Swift and Weinstein, 2009), further supporting the arterial identity of this vessel, as opposed to the rest of the components of the subintestinal basket (Fig. 1). In addition to the SIA, clear Notch-derived EGFP fluorescence was detected in a few cells within the retracting leading buds during the final stages of remodeling of the plexus (Fig. 7E, 60 hpf, arrows). These results are in line with the phenotypes resulting from DAPT treatment, and suggest that the role of Notch signaling is restricted to the late steps of resolution of the subintestinal angiogenic process, while it is dispensable for the earlier development of the plexus.

Interestingly, the ectopic SIV sprouts observed following DAPT treatment were reminiscent of those seen in *stalactite* (*stl*) mutants (Avraham-Davidi et al., 2012) (Fig 7F, arrows). In these embryos, ectopic angiogenesis results from the absence of apoprotein B (apoB)-containing lipoproteins, which in turn induces a significant reduction in the levels of the decoy receptor Vegfr1 (Flt1) (Avraham-Davidi et al., 2012). To analyze the putative involvement of Flt1 during formation of the subintestinal plexus, we downregulated both the membrane-, and soluble- isoforms of Flt1 using antisense morpholino oligonucleotides (MOs) (Zygmunt et al., 2011). While in WT siblings all leading buds have retracted by 3 dpf and a "clean" basket-shaped plexus is observed (Fig. 7A), these buds fail to remodel and retract following downregulation of Flt1 in either *stl* mutants, *mFlt1* or *sFlt1* morphants (Fig. 7F-H,

arrows, and 7I). Interestingly, *lyve1:dsRed* fluorescence was detected in the ectopic leading buds of both *stl* mutants and *flt1* morphants (Fig. S5), indicating that the venous identity of these sprouts is not dependent on Flt1. Altogether, these results suggest that Notch and Flt1 participate in the remodeling of the subintestinal plexus, which involves retraction of venous leading buds, but are not required for its initial development.

Molecular cues controlling the formation of the subintestinal vessels

The intricate paths involved in shaping the subintestinal vasculature prompted us to enquire into the molecular mechanisms underlying the different phases of this process. Since venous sprouting was shown to require VegfC signaling (Covassin et al., 2006; Kuchler et al., 2006; Hogan et al., 2009a) we examined the involvement of VegfC and Vegfr3/Flt4 in sprouting of ECs from the vPCV and formation of the subintestinal plexus. Analysis of *vegfc*^{um18} (Villefranc et al., 2013) and *flt4*^{um203} (Kok et al., 2015) mutants revealed no major defects in venous sprouting from the vPCV, or in the shape or length of the subintestinal basket (Fig. 8A-C), suggesting that the Vegfc-Flt4 axis does not play a major role in this process. Recently the BMP-signaling pathway has been implicated in sprouting from the axial vein (Wiley et al., 2011). Accordingly, we examined the role of BMP in shaping the subintestinal vasculature. We first analyzed BMP activity between 28 - 72 hpf in *Tg(2xBRE-AAVmlp:nlsmCherry)*, in which a BMP-responsive element (BRE) containing multiple Smad-binding sites induces expression of nuclear mCherry, in response to Smad 1/5/8 activation (Moro et al., 2013). Prior to ventral sprouting from the PCV, BMP-derived fluorescence was detected in EC-nuclei within the axial vessels (Fig. 8D, 28 hpf, arrowheads). Later on, clear labeling was seen in the primary SIV (Fig. 8D, 36hpf, arrowheads), and throughout the SIV and ICVs (Fig. 8D, 48-72 hpf, arrowheads). Nevertheless, no BMP activation was observed in the SIA. These results indicate the involvement of BMP signaling in ventral migration of the vPCV angioblasts, and in maintenance of venous fate of the SIV. In order to ascertain whether BMP is not only expressed in ECs forming the SIV, but also plays a role in this process, we examined the formation of the plexus in *Tg(fli1:EGFP;lyve1:dsRed;hsp70l:noggin3)* embryos, generated by mating *Tg(fli1:EGFP;lyve1:dsRed)* fish with the *Tg(hsp70l:noggin3)*^{fr13} (Chocron et al., 2007) line, in which forced expression of the BMP-antagonist *noggin3* is induced by heat-shock. While venous sprouting from the vPCV appears to occur normally in these embryos, as evident from the fact that a primary SIV is established at the relevant developmental stages, overexpression of *noggin3* completely inhibited the ventral migration of the subintestinal plexus, resulting in a significantly dorsalized basket (Fig. 8E,F). Interestingly, heat shock-induction of *noggin3* in *Tg(fli1:EGFP;lyve1:dsRed;hsp70l:noggin3)* embryos also resulted in loss of *lyve1*-derived dsRed fluorescence in the subintestinal basket of 82% of the treated embryos (Fig. 8E,G).

This effect may be attributed to a potential role for the BMP signaling pathway in induction/maintenance of venous fate in the vPCV angioblasts. Alternatively, reduction of *lyve1*-derived fluorescence in the SIV may reflect a different origin of the ECs forming these vessels, under *Noggin3* overexpression. To distinguish between these two possibilities we crossed *Tg(hsp70l:noggin3)* to *Tg(fli1:gal4;uas:kaede)* fish, heat-shocked their progeny at 26 hpf, and photoconverted the vPCV angioblasts at 30 hpf (Fig. 8H). At 55 hpf, the SIVs of both control and *noggin3*-overexpressing embryos displayed red fluorescence (Fig. 8I), suggesting that although the vPCV angioblasts are still able to leave the PCV and generate a primary SIV, they neither upregulate the expression of venous markers, nor engage in collective ventral migration, highlighting the BMP signaling pathway as a major player during the initial phases of formation of the subintestinal plexus.

"Arterial" signals control the development of the SIA

While ventral migration of the SIV was regulated by BMP, perturbations in this pathway had no apparent effect on formation of the SIA (Fig. 8E, arrows). We therefore decided to explore the involvement of well-established "arterial" circuits in formation of this vessel. We began by imaging *kdrl*^{y17} mutants, which carry a mutation in one of the zebrafish Vegf receptor-2 orthologs, previously shown to result in arterial-specific defects (Covassin et al., 2006). Assessment of the subintestinal plexus in these embryos revealed that both the sprouting of angioblasts from the vPCV, as well as the subsequent formation of the SIV take place normally (Movie 5). Yet, the subintestinal plexus of these embryos was characterized by a reduced number of ICVs as compared to their phenotypically WT siblings (Fig. 8J,K and Movie 5). These findings suggest a role for VEGF signaling in the "arterial" phase of the process, namely the dorsal migration of ECs from the SIV to generate the SIA. To further confirm this notion we analyzed the formation of the SIA in *plcg1*^{y10} mutants (Lawson et al., 2003), which lack Phospholipase C gamma-1 (*plcg*), a downstream effector of VEGF/Vegfr2 signaling (Takahashi et al., 2001). These mutants display clear defects in arterial development, but exhibit normal venous and lymphatic sprouting (Lawson et al., 2003; Lim et al., 2011; Nicenboim et al., 2015). The initial formation, as well as ventral migration of the SIV were normal in *plcg1* mutants (Movie 6), yet we detected a marked decrease in the number of ICVs and a complete absence of the SIA in all examined embryos (Fig 8J,K and Movie 6), indicating a key role for the *kdrl/plcg* axis in the dorsal migration phase of the subintestinal plexus formation.

DISCUSSION

We provide here a comprehensive study of the different steps underlying the formation of the zebrafish subintestinal plexus, and its relationship to the vascularization of the GI tract (Fig. 9). Our data track the embryonic origins, as well as the derivatives of each component of the subintestinal vessel network, and characterize the molecular circuits governing morphological changes that model the plexus into its final stereotypical shape. Serving as the primary source of the gastrointestinal vasculature, our results place the subintestinal plexus as an ideal model to study the interactions between organs and their specific vascular beds.

Using live imaging of transgenic zebrafish we show that formation of the subintestinal plexus takes place through ventral sprouting of specialized angioblasts from the floor of the PCV, which quickly anastomose and generate a primary SIV. EC-differentiation and collective ventral migration of the SIV is accompanied by incorporation of cells into the SIA, a phase that involves dorsal migration of single cells from the SIV. These findings highlight the plasticity of the vPCV angioblasts, and demonstrate their ability to generate not only arterial, venous and lymphatic ECs (Nicenboim et al., 2015), but also to contribute to mature vessels of at least three different organs (intestine, liver, pancreas), displaying significantly different features (Nolan et al., 2013).

Our previous results demonstrated that unpregulation of Prox1a in the vPCV angioblasts or in their progeny, determines their specification towards a lymphatic fate (Nicenboim et al., 2015). In contrast, we never detected Prox1a^{+} cells migrating ventrally to populate the subintestinal vessels (data not shown), highlighting the specific contribution of *prox1a*$^{+}$ cells to the lymphatic endothelium and not to other vascular beds. Based on these results, we postulate that the vPCV angioblasts bear the potential to generate multiple cell fates within the endothelial cascade. Yet, *in vivo*, they generate progeny based upon the signals to which they are exposed, and the specific developmental stage. Consequently, vPCV cells located in close proximity to the endoderm, are more likely to acquire a lymphatic fate following induction by the endoderm-secreted Wnt5b (Nicenboim et al., 2015), than vPCV cells which are located at more rostral positions, where the expression of Wnt5b is not detected. This hypothesis is further supported by the fact that as development proceeds there is a shift in the fate acquired by vPCV cells from population of PACs towards the subintestinal plexus (Nicenboim et al., 2015). Future experiments will be required to ascertain whether the vPCV angioblasts retain their plasticity as development proceeds, enabling the generation of different derivatives following exposure to diverse inducing signals.

Our genetic analyses show that ECs forming the subintestinal plexus respond to specific cues, which differentially guide their migration during each phase of the process. Through the use of genetic manipulations and transgenic reporters we demonstrate a clear role for the BMP signaling pathway in ventral migration and expansion of the plexus. Our data are in line with the findings reported by Wiley et al. (Wiley et al., 2011) showing that BMP signaling is necessary for the formation of the venous-derived caudal vein plexus (CVP). In this study, ECs cells in the CVP were shown to express the BMP receptors *bmpr2a* and *bmpr2b*, and to respond to BMP signaling. Furthermore, Bmp2b overexpression at 2.5 dpf, resulted in ectopic sprouts in the SIV suggesting that this vessel is responsive to BMP signaling (Wiley et al., 2011). In accordance with these results, we detect clear BMP activation in ECs of the SIV (Fig 8D), during the ventral migration and expansion of the basket. In contrast, while antagonizing BMP signaling inhibited the ability of sprouts from the axial vein to make connections and to form a proper CVP, BMP signaling was neither required for the initiation of vPCV ventral sprouting in the yolk area, nor for the establishment of a primitive SIV, thereby suggesting that this step is controlled by additional, yet unknown, molecular signals. Interestingly, forced overexpression of *noggin3* rendered a primary SIV that was not labeled by the lymph-venous marker *lyve1*, indicating an additional requirement for the BMP signaling pathway for proper specification/maintenance of venous fate in the vPCV angioblasts. We have recently identified the endoderm-secreted Wnt5b as a novel inductive signal promoting the 'angioblast-to-lymphatic' specification in the vPCV angioblasts (Nicenboim et al., 2015). In turn, Bmp2b has been shown to negatively regulate lymphatic cell fate specification (Dunworth et al., 2014), suggesting that the interplay between these two signaling pathways is instrumental for establishing the balance between venous vs. lymphatic ECs. The exact molecular mechanism underlying this crosstalk remains to be clarified.

While ventral migration of the SIV was BMP-dependent, dorsal migration of ECs from the SIV to generate the SIA was controlled by VEGF signaling. In both *kdrl* and *plcg1* mutants the number of ICVs was reduced, and severe defects were observed in the formation of the SIA. Interestingly, the dorsal migration of ECs from the SIV to generate the SIA, morphologically resemble the sprouting of arterial ISVs in the developing trunk (Isogai et al., 2003). Moreover, a common inhibitory effect over dorsal sprouting is seen in *kdrl* and *plcg1* mutants, in both the trunk ISVs (Lawson et al., 2003) and the ICVs of the subintestinal plexus (Fig. 8). This similarity is intriguing, considering that inhibition of Notch signaling affected the trunk-, and the subintestinal vasculature in different ways- while DAPT treatment induced increased number of ISV tip cells, dorsal sprouting from the SIV and formation of the ICVs was normal. Yet, reduced Notch signaling affected mainly the final steps of remodeling of the

subintestinal plexus, primarily inhibiting the retraction of the venous leading buds. This is in agreement with previous data, showing that Notch activation via overexpression of Dll4 results in reduction in the number of venous sprouts during secondary sprouting from the PCV (Hogan et al., 2009b). Similarly, Dll4-containing nucleosomes were shown to prompt Human Microvascular Endothelial Cells (HMVECs) to lose their filopodia and retract (Sharghi-Namini et al., 2014), supporting a differential role for Notch signaling during venous vs. arterial sprouting processes.

Given the molecular complexity of the circuits regulating the proper formation of the subintestinal plexus, it seems likely that additional factors, like blood circulation, may play a role in this process. While the role of blood flow during formation of the subintestinal plexus has remained controversial (Cermenati et al., 2008; Montero-Balaguer et al., 2009; Lenard et al., 2015), our preliminary data suggest that heart-beat arrest affects sprouting from the PCV and initial formation of the SIV (data not shown). Interestingly, in addition to the well established role of Notch signaling pathway in EC differentiation, specification, sprouting and migration (Phng and Gerhardt, 2009), it has also been shown to mediate the angiogenic effects of blood flow, including vessel identity and remodeling (Jones et al., 2006). Therefore, the subintestinal phenotypes resulting from the absence of blood flow, might potentially be mediated by Notch signaling. Alternatively, they could result from indirect, secondary effects caused by heart failure, and later on by hypoxia. Since the subintestinal plexus forms relatively late, as opposed to the primary intersegmental vessels that are only minimally affected by the lack of circulation, we cannot exclude the possibility that the second hypothesis is correct. Further *in vivo* experiments enabling to segregate between direct vs. indirect effects of absent blood flow will be required in order to answer this question

Our live imaging analyses revealed that ventral expansion of the plexus involves a phase of collective migration of the SIV via leading buds, which retract as the basket reaches its final shape. Interestingly, inhibition of both Notch and Flt1 activity resulted in the inability of the leading buds to retract. Impaired Notch signaling rendered embryos displaying ectopic SIV sprouts, as described following downregulation of the Notch ligand Delta-like 1 (Rodriguez et al., 2012). Moreover, our findings are in line with previous reports indicating the inhibitory effect of the Notch/Dll4 pathway on remodeling and regression of blood capillaries in the mouse retina model of oxygen-induced retinopathy (OIR) (Lobov et al., 2011). A role for Notch pathway in remodeling of the subintestinal plexus is further supported by the spatio-temporal pattern of Notch activity that was restricted to the SIA and to cells in leading buds, at a stage corresponding to remodeling of the plexus. In addition to Notch signaling, down regulation of both *mFlt1* and *sFlt1* resulted as well in the presence of ectopic leading buds along the SIV, in agreement with the phenotype of *stl* mutants (Avraham-Davidi

et al., 2012), suggesting a specific role for Flt1 in remodeling of the plexus through retraction of the leading buds. Altogether our results highlight certain similarities between the mechanisms underlying formation of the subintestinal plexus, and the "classic" process of tip/stalk cell coordination: 1. The angiogenic front is highly active, with extensive filopodial formation, 2. This process ceases once the vessels form and acquire their final shape. 3. There appears to be a feedback interaction between Notch and Vegf – loss of Notch and loss of Flt1 (similar to gain of Vegf) result in similar phenotypes. The main difference in the formation of these two vascular beds, resides in the particular cell behaviors – SIV formation involves a collective movement whereby a single vessel migrates as one unit, versus the traditional sprouting mechanism taking place during development of the trunk ISVs.

Interestingly, we found that the leading buds, which lead the collective ventral migration of the SIV, consisted mostly of two tip cells. These cells were found to overlap during most of the process of ventral expansion of the mature SIV. Similar results were reported for different sprouting assays including human umbilical endothelial cells (HUVECs), mouse retina, and mouse embryonic back vessels (Pelton et al., 2014). In all these cases, the majority of the angiogenic sprouts were shown to consist of two overlapping-, parallel cells, a phenomenon that could not be accounted for a transient overlap due to switch in position between the cells. In the future, it will be interesting to investigate whether this mechanism of vessel sprouting is specific for venous ECs. Our *in vivo* data support this idea and place the subintestinal plexus as an advantageous model for the study of this, and other cellular and molecular mechanisms controlling the interaction between tip/stalk and tip/tip cells during venous sprouting.

As a whole, the results presented here establish the subintestinal plexus as a model for the study of organ-specific vessel development. This process, which includes the specification of angioblasts towards venous and arterial fates, along with differential mechanisms of EC-migration and subsequent specification within a tissue-specific niche, is highly relevant to our understanding of blood vessel formation and wiring during disease states and tissue regeneration.

MATERIALS AND METHODS

Zebrafish husbandry and transgenic lines

Zebrafish were raised by standard methods (Avraham-Davidi et al., 2012) and handled according to the Weizmann Institute Animal Care and Use Committee. The *Tg(fli1:EGFP)*^{y1}, *Tg(fli1:nGFP*^{y7}*) (Yaniv et al., 2006), Tg(fli1:dsRed)*^{um1}(Covassin et al., 2009), *Tg(lyve1:dsRed2)*^{nz101} (Okuda et al., 2012), *Tg(fli1:gal4*^{ubs3}*;uasKaede*^{rk8}*)* (Herwig et al., 2011), *Tg(gata1a:dsRed)*^{sd2}(Yaniv et al., 2006), *vegfc*^{um18},(Villefranc et al., 2013) *Flt4*^{um203} (Kok et al., 2015), *Tg(hsp70l:noggin3)*^{fr13}(Chocron et al., 2007), *Tg(flt1_9a_cFos:GFP)*^{wz2} (Nicenboim et al., 2015), *Tg(gut:GFP)*^{s854} (Field et al., 2003a), *Tg(-1.0ins:EGFP)*^{sc1}(diIorio et al., 2002), *kdrl*^{y17}(Covassin et al., 2006), *Tg(2xBRE-AAVmlp:nlsmCherry)* (Moro et al., 2013) and *plcg1*^{y10} (Lawson et al., 2003) were described elsewhere. Genotypes of *vegfc*^{um18} and *Flt4*^{um203} mutants were verified as described before (Villefranc et al., 2013; Kok et al., 2015). The *Tg(fli1:LifeAct-GFP)*^{w4} was generated by cloning the LifeAct sequence (Riedl et al., 2008) into the TolFliepDest vector using the Gateway methodology (Villefranc et al., 2007). The Notch-responsive GFP reporter line, *Tg(EPV.Tp1-Mmu.Hbb:EGFP)*^{ia12} (12xNRE:EGFP) was generated by injection of a construct composed by six copies of the Epstein-Barr Virus Tp1 enhancer, each containing two Rbp-Jk binding sites, for a total of 12 Notch-responsive elements, placed in front of a murine beta-globin basal promoter driving EGFP (Parsons et al., 2009).

Manipulation of zebrafish embryos

Morpholino injection. The *sFlt1* 5'-GCCGCTATAAAGAATAAGGGCCTGA-3' (5ng), and *mFlt1* 5'-CAGCAGTTCACTCACATCTCCGTTC-3' (5ng) (Zygmunt et al., 2011) antisense morpholino oligonucleotides (Gene-tools) were resuspended and injected as described (Ben Shoham et al., 2012).

Heat-shock. 26 hpf *Tg(hsp70l:noggin3)* embryos were heat-shocked at 37°C for 40 minutes and scored for vascular phenotypes at 2 or 3 dpf. Genotyping was carried out using the Hsp70l forward primer (5'-CATGTGGACTGCCTATGTTCATC-3' and the *noggin3* reverse primer (5'-GGTGGCCAGGAAATACGGGATG-3').

DAPT experiments. Egg water containing DAPT was prepared by diluting fresh InSolution™ γ-Secretase Inhibitor IX (Merck Millipore) in fish water. Embryos were treated with 10 µM or 100 µM DAPT or DMSO (1:250) for the indicated time period and examined at 48 hpf or 72 hpf.

Photoswitching of *Tg(fli1:gal4;uasKaede)* embryos was performed using a 405 nm laser as described (Nicenboim et al., 2015). Embryos were analyzed at 24-48 hours after photoswitching. The percentage of embryos with red fluorescent cells in each vessel of the subintestinal plexus was calculated. Embryos with no fluorescence or with gross vascular morphological defects were excluded from quantification.

Quantifications of phenotypes including number of ICVs, number of ectopic SIV sprouts, sprout-length and length of the subintestinal basket (the distance between the vPCV and the bottom end of the SIV) were measured using ImageJ.

In situ hybridization

Tg(EPV.Tp1-Mmu.Hbb:EGFP) embryos were fixed in 4% PFA/PBS. The EGFP-specific antisense riboprobe was *in vitro* transcribed from an ApaI-linearized 383.pME-EGFP plasmid (Tol2kit), using T7 RNA polymerase and a DIG labeling kit (Roche). Whole-mount *in situ* hybridization was performed according to (Lauter et al., 2011). After flat mounting in 1% low melting agarose, far-red emission from Fast Blue-stained embryos (Sigma-Aldrich) was acquired.

Imaging

Confocal imaging was performed using a Zeiss LSM 780 upright confocal microscope (Carl Zeiss, Jena, Germany) with a W-Plan Apochromat ×20 objective, NA 1.0. Whole mount *in situ* hybridization images were acquired with a Leica SP5 spectral confocal microscope (633 nm laser line; 25x water dipping objective). Images of 12xNRE:EGFP embryos for EGFP intensity measurements were acquired using a Leica M165FC fluorescence microscope equipped with a Nikon DS-Fi2 camera. Images were processed using ImageJ (NIH), Volocity (PerkinElmer) and Imaris (Bitplane). Fluorescent proteins were excited sequentially with 488 nm and 563 nm single-photon lasers.

Time-lapse in-vivo imaging was performed as described (Nicenboim et al., 2015). z-stacks were acquired at 2.5–3 μm increments, every 9–16 minutes (shown in timestamp). For co-localization analyses, confocal images were analyzed using the Imaris ‘Co-localization Module’ and the Volocity 3D opacity utility. A new channel was applied to label with both EGFP and mCherry/dsRed fluorophores. Where necessary, movies were registered with the "Linear Stack Alignment with SIFT" plugin of FIJI. For the Notch reporter *Tg(EPV.Tp1-Mmu.Hbb:EGFP)* validation, quantification of EGFP protein fluoresence and mRNA levels (detected via Fast Blue-stained) was carried out using Volocity 6.0 software (Perkin Elmer). Quantification of EGFP florescence was performed on 50 um x 50 um regions of interest

(ROI) in the tail region, using the maximum pixel counting utility. Quantification of Fast Blue-stained fluorescence was performed on maximum projection files focusing on the hindbrain region (50 um x 50 um ROI), using the mean pixel counting utility.

Statistical analyses

Unpaired two-tailed Student's t-test assuming unequal variance from at least three independent experiments was used, unless stated otherwise. Numerical data are the mean ± s.e.m., unless stated otherwise.

ACKNOWLEDGMENTS

The authors would like to thank E. Raz for the *lifeact-GFP* plasmid. The authors are grateful to all the members of the Yaniv laboratory for discussion, technical assistance and continuous support. G.B. is a Junior Post-doc Fellow (CPDR124317/12) of the University of Padova, Italy. K.Y. is the incumbent of the Louis and Ida Rich Career Development Chair.

AUTHOR CONTRIBUTIONS STATEMENT

G.H. and J.N. designed and conducted experiments, analyzed data, and co-wrote the manuscript; L.A. and O.M. conducted experiments, and analyzed data; R.H. assisted with animal care; G.A. managed the fish facility; M.S. and N.D.L conducted experiments on *Vegfc* and *Flt4* mutants, analyzed data, and co-wrote the manuscript; N.T. and G.B. conducted experiments on *12xNRE:EGFP* and *Tg(2xBRE-AAVmlp:nlsmCherry)* reporters, and analyzed data ; K.Y. initiated and directed the study, designed experiments, analyzed data and co-wrote the paper with input from all authors.

COMPETING INTERESTS

The authors declare no competing or financial interests.

FUNDING

This work was supported in part by Marie Curie Actions-International Reintegration grants FP7-PEOPLE-2009-RG 256393 (to K.Y.), European Research Council 335605 (to K.Y.), Israel Science Foundation 861/13 (to K.Y.), Minerva Foundation 711128 (to K.Y.), and R01HL122599 from the National Heart, Lung, and Blood Institute (NHLBI; to N. D. L.). K.Y. is supported by the Willner Family Center for Vascular Biology; the estate of Paul Ourieff; the Carolito Stiftung; Lois Rosen, Los Angeles, CA; Edith Frumin; the Fondazione Henry Krenter; the Wallach Hanna & Georges Lustgarten Fund and the Polen Charitable Trust. N.T. is supported by the Italian Ministry of Health project Trambigen (RF-2010-2309484), the AFM-Telethon project Polygon (18572), the EU grant HEALTH-F4-2010-242048 “ZF-HEALTH: Zebrafish regulomics for human health”, and the UniPD grants Optozen (CPDA128151) and Tigre (CPDA148582/14).

REFERENCES

Adams, R. H. and Alitalo, K. (2007). Molecular regulation of angiogenesis and lymphangiogenesis. *Nature reviews. Molecular cell biology* **8**, 464-478.

Aird, W. C. (2007). Phenotypic heterogeneity of the endothelium: I. Structure, function, and mechanisms. *Circulation research* **100**, 158-173.

Avraham-Davidi, I., Ely, Y., Pham, V. N., Castranova, D., Grunspan, M., Malkinson, G., Gibbs-Bar, L., Mayseless, O., Allmog, G., Lo, B. et al. (2012). ApoB-containing lipoproteins regulate angiogenesis by modulating expression of VEGF receptor 1. *Nature medicine* **18**, 967-973.

Barbera-Guillem, E., Arrue, J. M., Ballesteros, J. and Vidal-Vanaclocha, F. (1986). Structural changes in endothelial cells of developing rat liver in the transition from fetal to postnatal life. *Journal of ultrastructure and molecular structure research* **97**, 197-206.

Ben Shoham, A., Malkinson, G., Krief, S., Shwartz, Y., Ely, Y., Ferrara, N., Yaniv, K. and Zelzer, E. (2012). S1P1 inhibits sprouting angiogenesis during vascular development. *Development* **139**, 3859-3869.

Braet, F. and Wisse, E. (2002). Structural and functional aspects of liver sinusoidal endothelial cell fenestrae: a review. *Comparative hepatology* **1**, 1.

Braet, F., De Zanger, R., Baekeland, M., Crabbe, E., Van Der Smissen, P. and Wisse, E. (1995). Structure and dynamics of the fenestrae-associated cytoskeleton of rat liver sinusoidal endothelial cells. *Hepatology* **21**, 180-189.

Cermenati, S., Moleri, S., Cimbro, S., Corti, P., Del Giacco, L., Amodeo, R., Dejana, E., Koopman, P., Cotelli, F. and Beltrame, M. (2008). Sox18 and Sox7 play redundant roles in vascular development. *Blood* **111**, 2657-2666.

Chocron, S., Verhoeven, M. C., Rentzsch, F., Hammerschmidt, M. and Bakkers, J. (2007). Zebrafish Bmp4 regulates left-right asymmetry at two distinct developmental time points. *Developmental biology* **305**, 577-588.

Cleaver, O. (2004). Blood vessel signals during development and beyond. *Current topics in developmental biology* **62**, 1-36.

Covassin, L. D., Villefranc, J. A., Kacergis, M. C., Weinstein, B. M. and Lawson, N. D. (2006). Distinct genetic interactions between multiple Vegf receptors are required for development of different blood vessel types in zebrafish. *Proceedings of the National Academy of Sciences of the United States of America* **103**, 6554-6559.

Covassin, L. D., Siekmann, A. F., Kacergis, M. C., Laver, E., Moore, J. C., Villefranc, J. A., Weinstein, B. M. and Lawson, N. D. (2009). A genetic screen for vascular mutants in zebrafish reveals dynamic roles for Vegf/Plcg1 signaling during artery development. *Developmental biology* **329**, 212-226.

dilorio, P. J., Moss, J. B., Sbrogna, J. L., Karlstrom, R. O. and Moss, L. G. (2002). Sonic hedgehog is required early in pancreatic islet development. *Developmental biology* **244**, 75-84.

Ding, B. S., Cao, Z., Lis, R., Nolan, D. J., Guo, P., Simons, M., Penfold, M. E., Shido, K., Rabbany, S. Y. and Rafii, S. (2014). Divergent angiocrine signals from vascular niche balance liver regeneration and fibrosis. *Nature* **505**, 97-102.

Ding, B. S., Nolan, D. J., Butler, J. M., James, D., Babazadeh, A. O., Rosenwaks, Z., Mittal, V., Kobayashi, H., Shido, K., Lyden, D. et al. (2010). Inductive angiocrine signals from sinusoidal endothelium are required for liver regeneration. *Nature* **468**, 310-315.

Dunworth, W. P., Cardona-Costa, J., Bozkulak, E. C., Kim, J. D., Meadows, S., Fischer, J. C., Wang, Y., Cleaver, O., Qyang, Y., Ober, E. A. et al. (2014). Bone morphogenetic protein 2

signaling negatively modulates lymphatic development in vertebrate embryos. *Circulation research* **114**, 56-66.
Edlund, H. (2002). Pancreatic organogenesis--developmental mechanisms and implications for therapy. *Nature reviews. Genetics* **3**, 524-532.
Field, H. A., Ober, E. A., Roeser, T. and Stainier, D. Y. (2003a). Formation of the digestive system in zebrafish. I. Liver morphogenesis. *Developmental biology* **253**, 279-290.
Field, H. A., Dong, P. D., Beis, D. and Stainier, D. Y. (2003b). Formation of the digestive system in zebrafish. II. Pancreas morphogenesis. *Developmental biology* **261**, 197-208.
Fujita, M., Isogai, S. and Kudo, A. (2006). Vascular anatomy of the developing medaka, Oryzias latipes: a complementary fish model for cardiovascular research on vertebrates. *Developmental dynamics : an official publication of the American Association of Anatomists* **235**, 734-746.
Gerhardt, H., Golding, M., Fruttiger, M., Ruhrberg, C., Lundkvist, A., Abramsson, A., Jeltsch, M., Mitchell, C., Alitalo, K., Shima, D. et al. (2003). VEGF guides angiogenic sprouting utilizing endothelial tip cell filopodia. *The Journal of cell biology* **161**, 1163-1177.
Helker, C. S., Schuermann, A., Karpanen, T., Zeuschner, D., Belting, H. G., Affolter, M., Schulte-Merker, S. and Herzog, W. (2013). The zebrafish common cardinal veins develop by a novel mechanism: lumen ensheathment. *Development* **140**, 2776-2786.
Hellstrom, M., Phng, L. K., Hofmann, J. J., Wallgard, E., Coultas, L., Lindblom, P., Alva, J., Nilsson, A. K., Karlsson, L., Gaiano, N. et al. (2007). Dll4 signalling through Notch1 regulates formation of tip cells during angiogenesis. *Nature* **445**, 776-780.
Herwig, L., Blum, Y., Krudewig, A., Ellertsdottir, E., Lenard, A., Belting, H. G. and Affolter, M. (2011). Distinct cellular mechanisms of blood vessel fusion in the zebrafish embryo. *Current biology : CB* **21**, 1942-1948.
Hogan, B. M., Bos, F. L., Bussmann, J., Witte, M., Chi, N. C., Duckers, H. J. and Schulte-Merker, S. (2009a). Ccbe1 is required for embryonic lymphangiogenesis and venous sprouting. *Nature genetics* **41**, 396-398.
Hogan, B. M., Herpers, R., Witte, M., Helotera, H., Alitalo, K., Duckers, H. J. and Schulte-Merker, S. (2009b). Vegfc/Flt4 signalling is suppressed by Dll4 in developing zebrafish intersegmental arteries. *Development* **136**, 4001-4009.
Hu, J., Srivastava, K., Wieland, M., Runge, A., Mogler, C., Besemfelder, E., Terhardt, D., Vogel, M. J., Cao, L., Korn, C. et al. (2014). Endothelial cell-derived angiopoietin-2 controls liver regeneration as a spatiotemporal rheostat. *Science* **343**, 416-419.
Isogai, S., Horiguchi, M. and Weinstein, B. M. (2001). The vascular anatomy of the developing zebrafish: an atlas of embryonic and early larval development. *Developmental biology* **230**, 278-301.
Isogai, S., Lawson, N. D., Torrealday, S., Horiguchi, M. and Weinstein, B. M. (2003). Angiogenic network formation in the developing vertebrate trunk. *Development* **130**, 5281-5290.
Jakobsson, L., Franco, C. A., Bentley, K., Collins, R. T., Ponsioen, B., Aspalter, I. M., Rosewell, I., Busse, M., Thurston, G., Medvinsky, A. et al. (2010). Endothelial cells dynamically compete for the tip cell position during angiogenic sprouting. *Nature cell biology* **12**, 943-953.
Jones, E. A., le Noble, F. and Eichmann, A. (2006). What determines blood vessel structure? Genetic prespecification vs. hemodynamics. *Physiology* **21**, 388-395.
Kim, S. K. and Hebrok, M. (2001). Intercellular signals regulating pancreas development and function. *Genes & development* **15**, 111-127.
Kok, F. O., Shin, M., Ni, C. W., Gupta, A., Grosse, A. S., van Impel, A., Kirchmaier, B. C., Peterson-Maduro, J., Kourkoulis, G., Male, I. et al. (2015). Reverse genetic screening reveals poor correlation between morpholino-induced and mutant phenotypes in zebrafish. *Developmental cell* **32**, 97-108.

Korzh, S., Pan, X., Garcia-Lecea, M., Winata, C. L., Pan, X., Wohland, T., Korzh, V. and Gong, Z. (2008). Requirement of vasculogenesis and blood circulation in late stages of liver growth in zebrafish. *BMC developmental biology* **8**, 84.
Kuchler, A. M., Gjini, E., Peterson-Maduro, J., Cancilla, B., Wolburg, H. and Schulte-Merker, S. (2006). Development of the zebrafish lymphatic system requires VEGFC signaling. *Current biology : CB* **16**, 1244-1248.
Lammert, E., Cleaver, O. and Melton, D. (2001). Induction of pancreatic differentiation by signals from blood vessels. *Science* **294**, 564-567.
Lammert, E., Cleaver, O. and Melton, D. (2003). Role of endothelial cells in early pancreas and liver development. *Mechanisms of development* **120**, 59-64.
Lauter, G., Soll, I. and Hauptmann, G. (2011). Two-color fluorescent in situ hybridization in the embryonic zebrafish brain using differential detection systems. *BMC developmental biology* **11**, 43.
Lawson, N. D. and Weinstein, B. M. (2002). Arteries and veins: making a difference with zebrafish. *Nature reviews. Genetics* **3**, 674-682.
Lawson, N. D., Mugford, J. W., Diamond, B. A. and Weinstein, B. M. (2003). phospholipase C gamma-1 is required downstream of vascular endothelial growth factor during arterial development. *Genes & development* **17**, 1346-1351.
Lawson, N. D., Scheer, N., Pham, V. N., Kim, C. H., Chitnis, A. B., Campos-Ortega, J. A. and Weinstein, B. M. (2001). Notch signaling is required for arterial-venous differentiation during embryonic vascular development. *Development* **128**, 3675-3683.
Lenard, A., Daetwyler, S., Betz, C., Ellertsdottir, E., Belting, H. G., Huisken, J. and Affolter, M. (2015). Endothelial Cell Self-fusion during Vascular Pruning. *PLoS biology* **13**, e1002126.
Leslie, J. D., Ariza-McNaughton, L., Bermange, A. L., McAdow, R., Johnson, S. L. and Lewis, J. (2007). Endothelial signalling by the Notch ligand Delta-like 4 restricts angiogenesis. *Development* **134**, 839-844.
Lim, A. H., Suli, A., Yaniv, K., Weinstein, B., Li, D. Y. and Chien, C. B. (2011). Motoneurons are essential for vascular pathfinding. *Development* **138**, 3847-3857.
Lobov, I. B., Cheung, E., Wudali, R., Cao, J., Halasz, G., Wei, Y., Economides, A., Lin, H. C., Papadopoulos, N., Yancopoulos, G. D. et al. (2011). The Dll4/Notch pathway controls postangiogenic blood vessel remodeling and regression by modulating vasoconstriction and blood flow. *Blood* **117**, 6728-6737.
Matsumoto, K., Yoshitomi, H., Rossant, J. and Zaret, K. S. (2001). Liver organogenesis promoted by endothelial cells prior to vascular function. *Science* **294**, 559-563.
Montero-Balaguer, M., Swirsding, K., Orsenigo, F., Cotelli, F., Mione, M. and Dejana, E. (2009). Stable vascular connections and remodeling require full expression of VE-cadherin in zebrafish embryos. *PloS one* **4**, e5772.
Moro, E., Vettori, A., Porazzi, P., Schiavone, M., Rampazzo, E., Casari, A., Ek, O., Facchinello, N., Astone, M., Zancan, I. et al. (2013). Generation and application of signaling pathway reporter lines in zebrafish. *Molecular genetics and genomics : MGG* **288**, 231-242.
Murtaugh, L. C. (2007). Pancreas and beta-cell development: from the actual to the possible. *Development* **134**, 427-438.
Ng, A. N., de Jong-Curtain, T. A., Mawdsley, D. J., White, S. J., Shin, J., Appel, B., Dong, P. D., Stainier, D. Y. and Heath, J. K. (2005). Formation of the digestive system in zebrafish: III. Intestinal epithelium morphogenesis. *Developmental biology* **286**, 114-135.
Nicenboim, J., Malkinson, G., Lupo, T., Asaf, L., Sela, Y., Mayseless, O., Gibbs-Bar, L., Senderovich, N., Hashimshony, T., Shin, M. et al. (2015). Lymphatic vessels arise from specialized angioblasts within a venous niche. *Nature* **522**, 56-61.
Nicoli, S. and Presta, M. (2007). The zebrafish/tumor xenograft angiogenesis assay. *Nature protocols* **2**, 2918-2923.

Nikolova, G. and Lammert, E. (2003). Interdependent development of blood vessels and organs. *Cell and tissue research* **314**, 33-42.
Nolan, D. J., Ginsberg, M., Israely, E., Palikuqi, B., Poulos, M. G., James, D., Ding, B. S., Schachterle, W., Liu, Y., Rosenwaks, Z. et al. (2013). Molecular signatures of tissue-specific microvascular endothelial cell heterogeneity in organ maintenance and regeneration. *Developmental cell* **26**, 204-219.
Ober, E. A., Field, H. A. and Stainier, D. Y. (2003). From endoderm formation to liver and pancreas development in zebrafish. *Mechanisms of development* **120**, 5-18.
Okuda, K. S., Astin, J. W., Misa, J. P., Flores, M. V., Crosier, K. E. and Crosier, P. S. (2012). lyve1 expression reveals novel lymphatic vessels and new mechanisms for lymphatic vessel development in zebrafish. *Development* **139**, 2381-2391.
Parsons, M. J., Pisharath, H., Yusuff, S., Moore, J. C., Siekmann, A. F., Lawson, N. and Leach, S. D. (2009). Notch-responsive cells initiate the secondary transition in larval zebrafish pancreas. *Mechanisms of development* **126**, 898-912.
Pelton, J. C., Wright, C. E., Leitges, M. and Bautch, V. L. (2014). Multiple endothelial cells constitute the tip of developing blood vessels and polarize to promote lumen formation. *Development* **141**, 4121-4126.
Phng, L. K. and Gerhardt, H. (2009). Angiogenesis: a team effort coordinated by notch. *Developmental cell* **16**, 196-208.
Phng, L. K., Stanchi, F. and Gerhardt, H. (2013). Filopodia are dispensable for endothelial tip cell guidance. *Development* **140**, 4031-4040.
Potente, M., Gerhardt, H. and Carmeliet, P. (2011). Basic and therapeutic aspects of angiogenesis. *Cell* **146**, 873-887.
Quillien, A., Moore, J. C., Shin, M., Siekmann, A. F., Smith, T., Pan, L., Moens, C. B., Parsons, M. J. and Lawson, N. D. (2014). Distinct Notch signaling outputs pattern the developing arterial system. *Development* **141**, 1544-1552.
Riedl, J., Crevenna, A. H., Kessenbrock, K., Yu, J. H., Neukirchen, D., Bista, M., Bradke, F., Jenne, D., Holak, T. A., Werb, Z. et al. (2008). Lifeact: a versatile marker to visualize F-actin. *Nature methods* **5**, 605-607.
Rodriguez, P., Higueras, M. A., Gonzalez-Rajal, A., Alfranca, A., Fierro-Fernandez, M., Garcia-Fernandez, R. A., Ruiz-Hidalgo, M. J., Monsalve, M., Rodriguez-Pascual, F., Redondo, J. M. et al. (2012). The non-canonical NOTCH ligand DLK1 exhibits a novel vascular role as a strong inhibitor of angiogenesis. *Cardiovascular research* **93**, 232-241.
Sakaguchi, T. F., Sadler, K. C., Crosnier, C. and Stainier, D. Y. (2008). Endothelial signals modulate hepatocyte apicobasal polarization in zebrafish. *Current biology : CB* **18**, 1565-1571.
Serbedzija, G. N., Flynn, E. and Willett, C. E. (1999). Zebrafish angiogenesis: a new model for drug screening. *Angiogenesis* **3**, 353-359.
Sharghi-Namini, S., Tan, E., Ong, L. L., Ge, R. and Asada, H. H. (2014). Dll4-containing exosomes induce capillary sprout retraction in a 3D microenvironment. *Scientific reports* **4**, 4031.
Siekmann, A. F. and Lawson, N. D. (2007). Notch signalling limits angiogenic cell behaviour in developing zebrafish arteries. *Nature* **445**, 781-784.
Suli, A., Mortimer, N., Shepherd, I. and Chien, C. B. (2006). Netrin/DCC signaling controls contralateral dendrites of octavolateralis efferent neurons. *The Journal of neuroscience : the official journal of the Society for Neuroscience* **26**, 13328-13337.
Swift, M. R. and Weinstein, B. M. (2009). Arterial-venous specification during development. *Circulation research* **104**, 576-588.
Takahashi, T., Yamaguchi, S., Chida, K. and Shibuya, M. (2001). A single autophosphorylation site on KDR/Flk-1 is essential for VEGF-A-dependent activation of PLC-gamma and DNA synthesis in vascular endothelial cells. *The EMBO journal* **20**, 2768-2778.

Torres-Vazquez, J., Gitler, A. D., Fraser, S. D., Berk, J. D., Van, N. P., Fishman, M. C., Childs, S., Epstein, J. A. and Weinstein, B. M. (2004). Semaphorin-plexin signaling guides patterning of the developing vasculature. *Developmental cell* **7**, 117-123.
Villefranc, J. A., Amigo, J. and Lawson, N. D. (2007). Gateway compatible vectors for analysis of gene function in the zebrafish. *Developmental dynamics : an official publication of the American Association of Anatomists* **236**, 3077-3087.
Villefranc, J. A., Nicoli, S., Bentley, K., Jeltsch, M., Zarkada, G., Moore, J. C., Gerhardt, H., Alitalo, K. and Lawson, N. D. (2013). A truncation allele in vascular endothelial growth factor c reveals distinct modes of signaling during lymphatic and vascular development. *Development* **140**, 1497-1506.
Wallace, K. N. and Pack, M. (2003). Unique and conserved aspects of gut development in zebrafish. *Developmental biology* **255**, 12-29.
Wiley, D. M., Kim, J. D., Hao, J., Hong, C. C., Bautch, V. L. and Jin, S. W. (2011). Distinct signalling pathways regulate sprouting angiogenesis from the dorsal aorta and the axial vein. *Nature cell biology* **13**, 686-692.
Yaniv, K., Isogai, S., Castranova, D., Dye, L., Hitomi, J. and Weinstein, B. M. (2006). Live imaging of lymphatic development in the zebrafish. *Nature medicine* **12**, 711-716.
Yoshitomi, H. and Zaret, K. S. (2004). Endothelial cell interactions initiate dorsal pancreas development by selectively inducing the transcription factor Ptf1a. *Development* **131**, 807-817.
Zygmunt, T., Gay, C. M., Blondelle, J., Singh, M. K., Flaherty, K. M., Means, P. C., Herwig, L., Krudewig, A., Belting, H. G., Affolter, M. et al. (2011). Semaphorin-PlexinD1 signaling limits angiogenic potential via the VEGF decoy receptor sFlt1. *Developmental cell* **21**, 301-314.

Figures

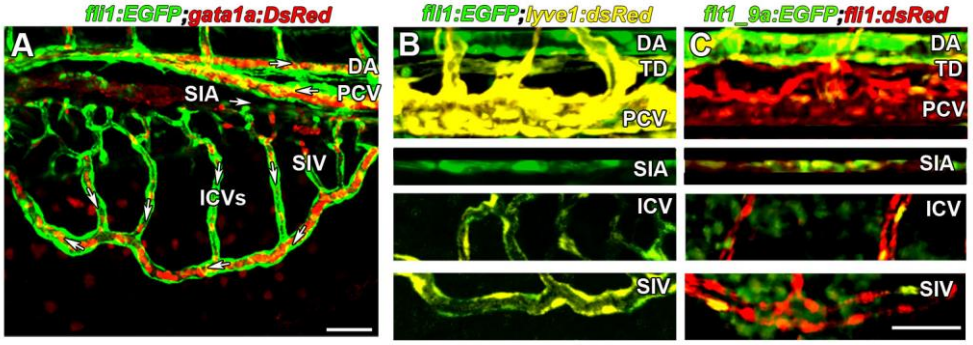

Figure 1. Arterial-venous identity of the subintestinal vessels

A. Directionality of blood flow in the subintestinal plexus, as determined in *Tg(fli1:EGFP;gata1a:dsRed)* embryo at 3.5 dpf. White arrows indicate the direction of flow in the DA, PCV, SIA, SIV, and ICVs. **B.** Colocalization (yellow) of *fli1:EGFP* (green)-, and *lyve1:dsRed*- fluorescence in venous ECs of the PCV, ICVs, TD and SIV of 4 dpf *Tg(fli1:EGFP; lyve1:dsRed)* double transgenic embryos. The DA and SIA show no *lyve1:dsRed* expression. **C.** Colocalization (yellow) of *fli1*:*dsRed*-, and *flt1_9a* (green)- in arterial ECs of the DA and SIA of 4 dpf *Tg(flt1_9a_cfos:GFP; fli1:dsRed)* double transgenic embryos. DA, dorsal aorta; ICVs, inter-connecting vessels; PCV, posterior cardinal vein; SIA, supraintestinal artery; SIV, subintestinal vein; TD, thoracic duct. Scale bar: 50 µm.

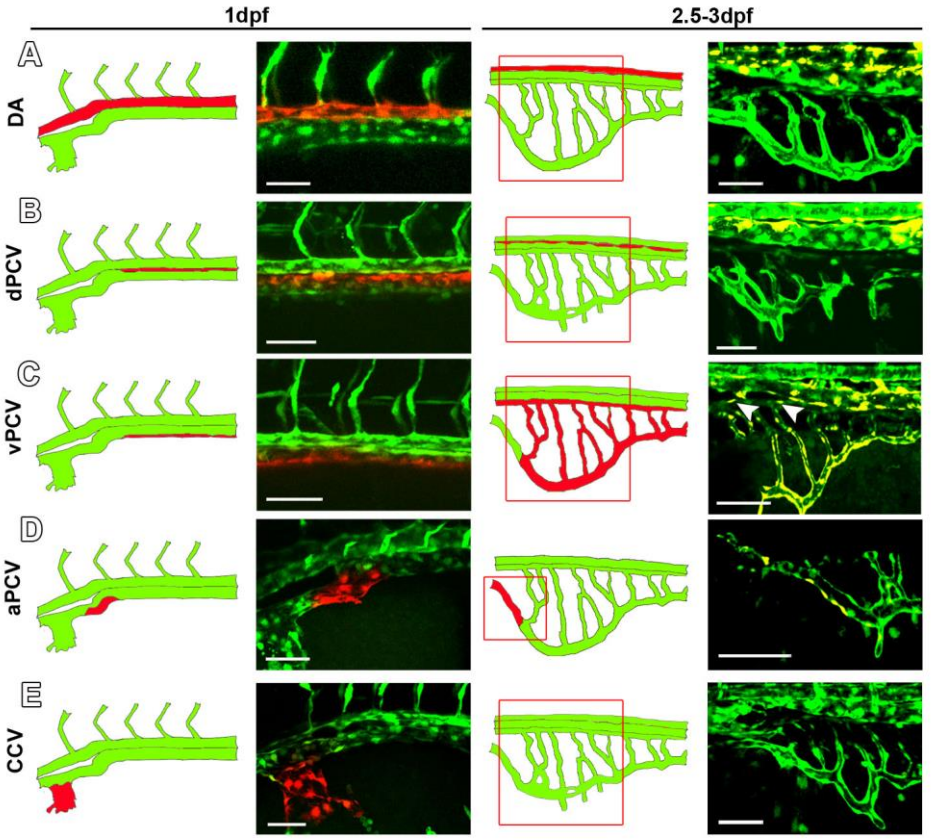

Figure 2. PCV cells give rise to all components of the subintestinal plexus

A-E. Photoswitching of selected ECs was performed at 1dpf in *Tg(fli1:gal4;uas:kaede)* embryos, and vessels were scored for the presence of red-labeled ECs at 2.5-3 dpf. Schematic illustrations of the corresponding confocal images are shown to the left. No photoconverted red-cells were detected in the subintestinal plexus following photoswitching of the DA (**A**), dPCV (**B**) and CCV (**E**). Photoswitching of the vPCV (**C**) rendered red-labeled ECs in all components of the subintestinal plexus, including the SIA (arrowheads), whereas photoconverted ECs from the aPCV (**D**) were found exclusively in the rostral most part of the SIV. CCV, common cardinal vein; DA, dorsal aorta; aPCV, anterior PCV; SIV, subintestinal vein; dPCV, dorsal PCV; vPCV, ventral PCV. Scale bar: 50 µm. n_{DA}=24, n_{dPCV}=10, n_{vPCV}=16, n_{aPCV}=5, n_{CCV}=11.

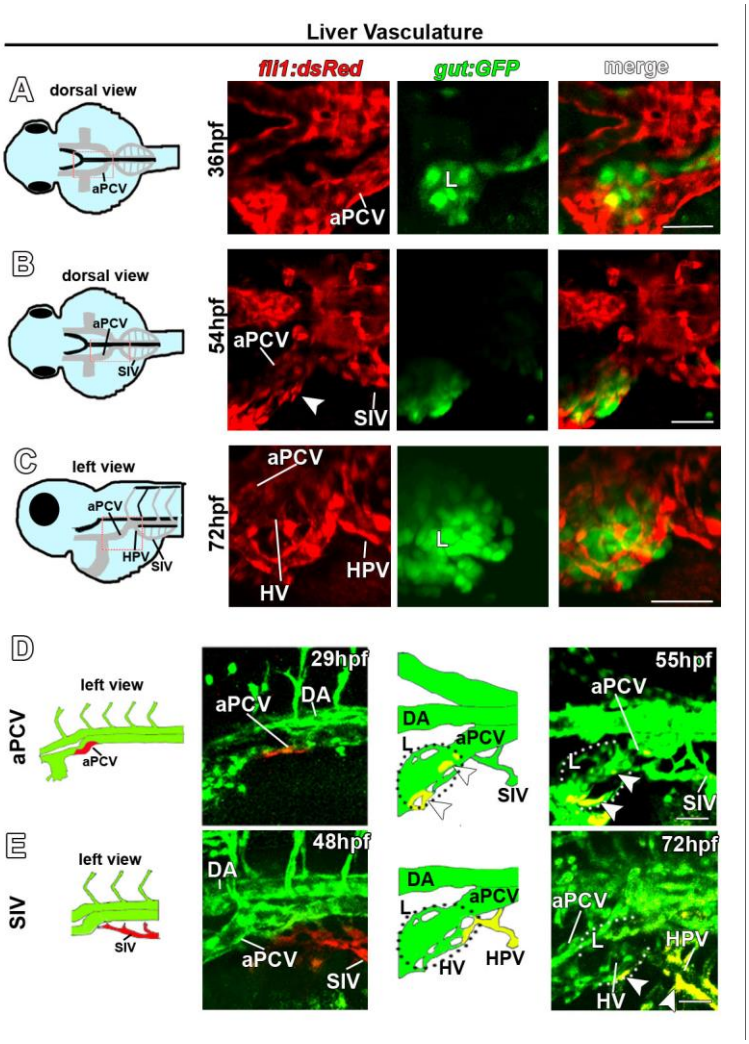

Figure 3: The left subintestinal vein and aPCV give rise to the liver vasculature

A-C. Confocal images of *Tg(gut:GFP;fli1:dsRed)* double transgenic embryos at 36-72 hpf highlighting the vasculature (red) and the liver (L, green). **A**. The aPCV on the left side of the embryo is found adjacent to the liver at 36 hpf. **B,C**. ECs surround the liver by 54hpf (**B,** arrowhead), and form the hepatic vessels (HV) by 72 hpf (**C**). The SIV drains into the liver via the HPV (**C**). **D,E** Photoswitching of ECs in the left branch of the aPCV (**D**), or the left SIV (**E**) was performed at 29 hpf in *Tg(fli1:gal4;uas:kaede)* embryos. **D**. Red-labeled ECs from the left aPCV contribute to the liver vasculature (55hpf, arrowheads). **E.** Photoswitching of the left SIV at 48hpf rendered red-labeled ECs in the HVs and the HPV (**E,** 72 hpf, arrowheads). aPCV, anterior PCV; DA, dorsal aorta; HPV, hepatic portal vein; HV, hepaic vessels; L, liver; SIV, subintestinal vein. Scale bar, 50µm. $n_{aPCV}=4$, $n_{siv}=5$

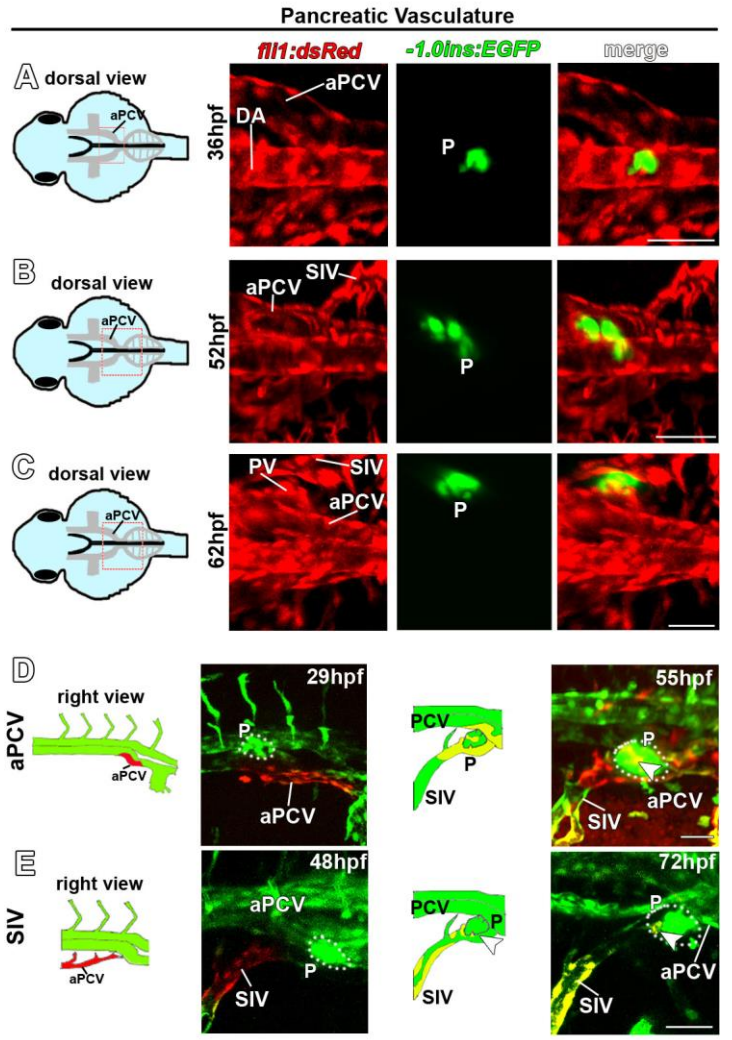

Figure 4: The right subintestinal vein and aPCV give rise to the pancreatic vasculature

A-C. Confocal images of *Tg(-1.0ins:EGFP;fli1:dsRed)* embryos at 36-62 hpf highlighting the vasculature and the endocrine pancreas (green). **A**. *insulin:EGFP*$^{+}$ cells are detected between the two branches of the aPCV at 36hpf. **B,C**. Gradual shift of *insulin:EGFP*$^{+}$ cells towards the right side of the midline. **C**. The most cranial ICV on the right side of the plexus (**C**, 62 hpf) sends branches towards the nascent pancreas. **D,E** Photoswitching of ECs in the right branch of the aPCV at 29 hpf (**D**) or in the right SIV at 48 hpf (**E**) was performed in *Tg(fli1:gal4;uas:kaede; -1.0ins:EGFP*) embryos. **D**. Red-labeled ECs from the right aPCV contribute to the pancreatic vasculature (55hpf, arrowhead). **E**. Photoswitching of the right SIV at 48hpf rendered red-labeled ECs in the pancreatic vasculature (72 hpf, arrowheads). aPCV, anterior PCV; DA, dorsal aorta; P, pancreas; PV, pancreatic vessels; SIV, subintestinal vein. Scale bar, 50µm. n_{aPCV}=8, n_{siv}=11

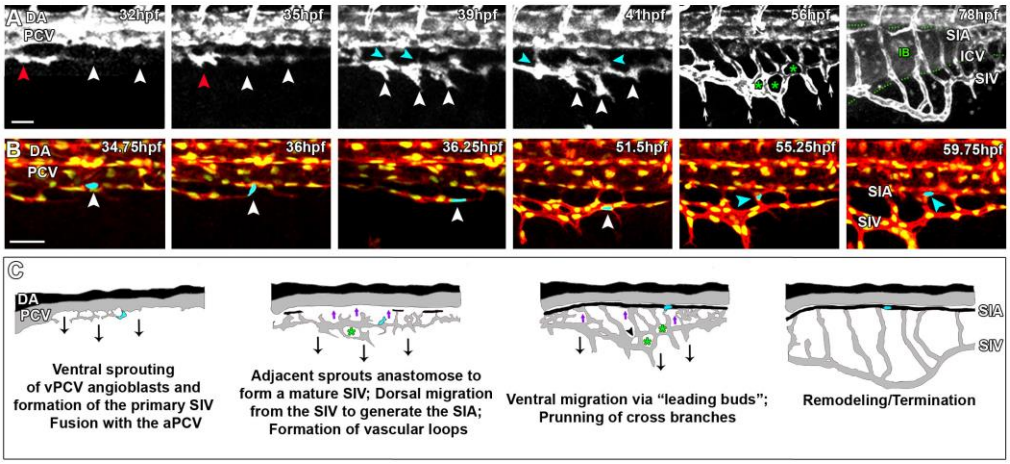

Figure 5. Formation of the subintestinal plexus involves different mechanisms of EC-migration

A. Snapshots from a time-lapse sequence of a *Tg(fli1:dsRed)* embryo, showing individual sprouts arising from the vPCV (32 hpf, white arrowheads), which quickly anastomose and fuse with a caudal projection of the aPCV (red arrowhead) to generate the primary SIV. Sprouts arising along the primary SIV elongate ventrally and fuse to generate the mature SIV (35-41 hpf, white arrowheads). Concomitantly, ECs from the SIV migrate dorsally to generate the SIA (39-41 hpf, light-blue arrowheads). The mature SIV migrates ventrally through leading buds-guided collective migration (56 hpf, white arrows), while fusion of angiogenic sprouts originating in the primary SIV generate vascular loops (56 hpf, green asterisks). Leading buds retraction, along with pruning of the cross branches forming the vascular loops, render the stereotypical basket shape (78 hpf) that engulfs the intestinal bulb (IB). **B.** Snapshots from a time-lapse sequence of a *Tg(fli1:dsRed;fli1:nGFP)* showing the migration route taken by vPCV angioblasts. A single angioblast (light-blue) initially residing in the vPCV (34.75 hpf, white arrowhead) sprouts ventrally (36 hpf, white arrowhead) and incorporates into the primary SIV (36.25 - 51.5 hpf, white arrowhead). Later on, the same cell lags-back shortly and migrates dorsally (55.25 hpf, light-blue arrowhead) eventually incorporating into the SIA (59.75 hpf, light-blue arrowhead). **C.** Schematic illustration depicting the different steps involved in formation of the subintestinal plexus. Ventral sprouting and ventral migration (black arrows), cells "lagging-back" followed by dorsal migration (purple arrows), vascular loops (green asterisks), and vessel pruning (black arrowhead). DA, dorsal aorta; IB, intestinal bulb; ICVs, inter-connecting vessels; PCV, posterior cardinal vein; SIA, supraintestinal artery; SIV, subintestinal vein. Scale bar: 50 µm.

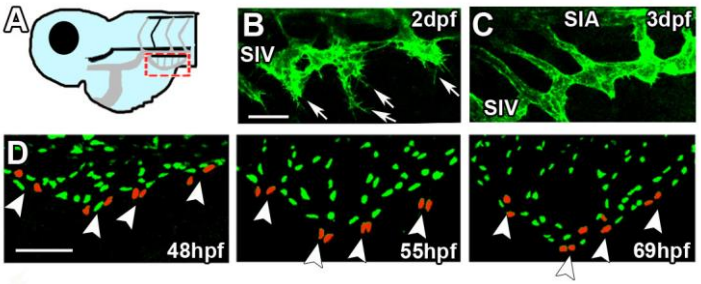

Figure 6. Establishment of the SIV involves leading bud-guided collective migration of ECs

A. Box on diagram shows approximate location of regions imaged in panels **B-D**. **B.** Actin-rich filopodia (arrows) are detected at the SIV migration-front in *Tg(lifeact:GFP)* embryos at 2 dpf. **C**. As the plexus reaches its stereotypical basket shape at 3 dpf, all filopodia retract. **D.** Distribution of EC-nuclei in *Tg(fli1:nGFP)* embryos demonstrates that leading buds consist of paired ECs (48-55 hpf, arrowheads), rather than of a single tip cell. Towards the end of the process, leading buds retract and incorporate into the SIV (69 hpf, arrowheads). SIA, supraintestinal artery; SIV, subintestinal vein. Scale bar: 50 µm.

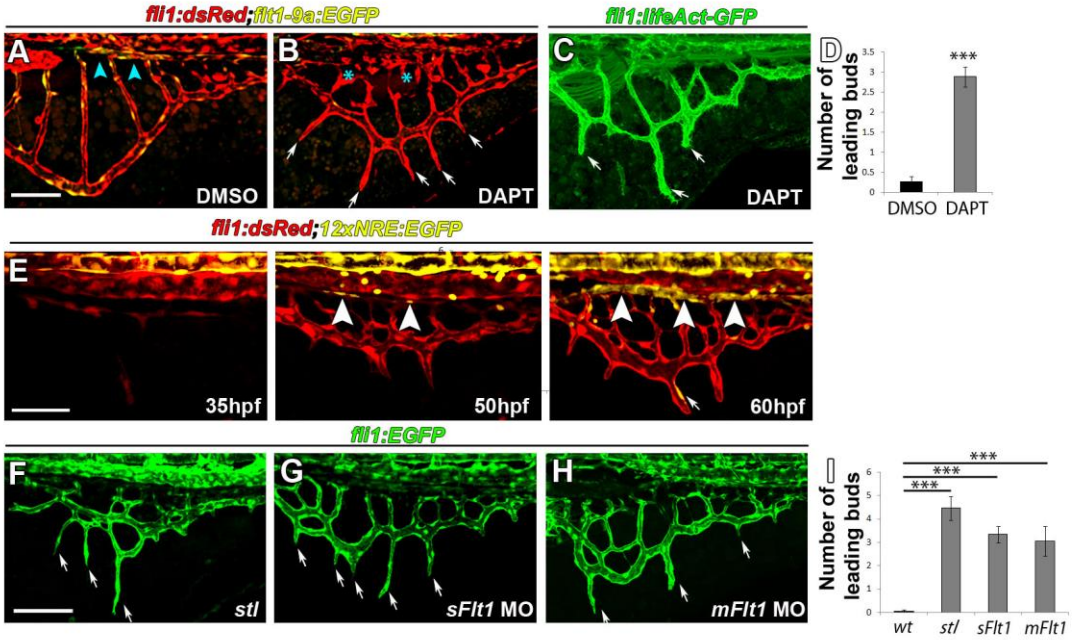

Figure 7. Notch activity is required for final remodeling of the subintestinal plexus but is dispensable for its initial development

A-D. The subintestinal plexus of 72 hpf *Tg(fli1:dsRed; flt1_9a_cFos:GFP)* embryos treated with DAPT between 24-72 hpf shows the presence of ectopic leading buds (**B**, **C,** arrows, **D**), malformed SIA (**B**, asterisks), and active filopodia along the SIV (**C**). **E**. Spatio-temporal characterization of Notch signaling activation during development of the subintestinal plexus, as detected in *Tg(fli1:dsRed;12xNRE:EGFP)* double transgenic embryos. EGFP is detected in the SIA starting at 50 hpf (arrowheads), and in the leading-buds of 60 hpf embryos (arrow). **F-I.** Downregulation of *flt1* results in ectopic leading buds along the SIV of *stl* mutants (**F,** arrows), *sFlt1* (**G,** arrows), and *mFlt1* (**H**, arrows) morphants, quantified in **I**. Scale bar: 50 µm. n_{Ctrl}=16, n_{stl}=13, n_{mFlt}=27, n_{sFlt}=18. ***P<0.001.

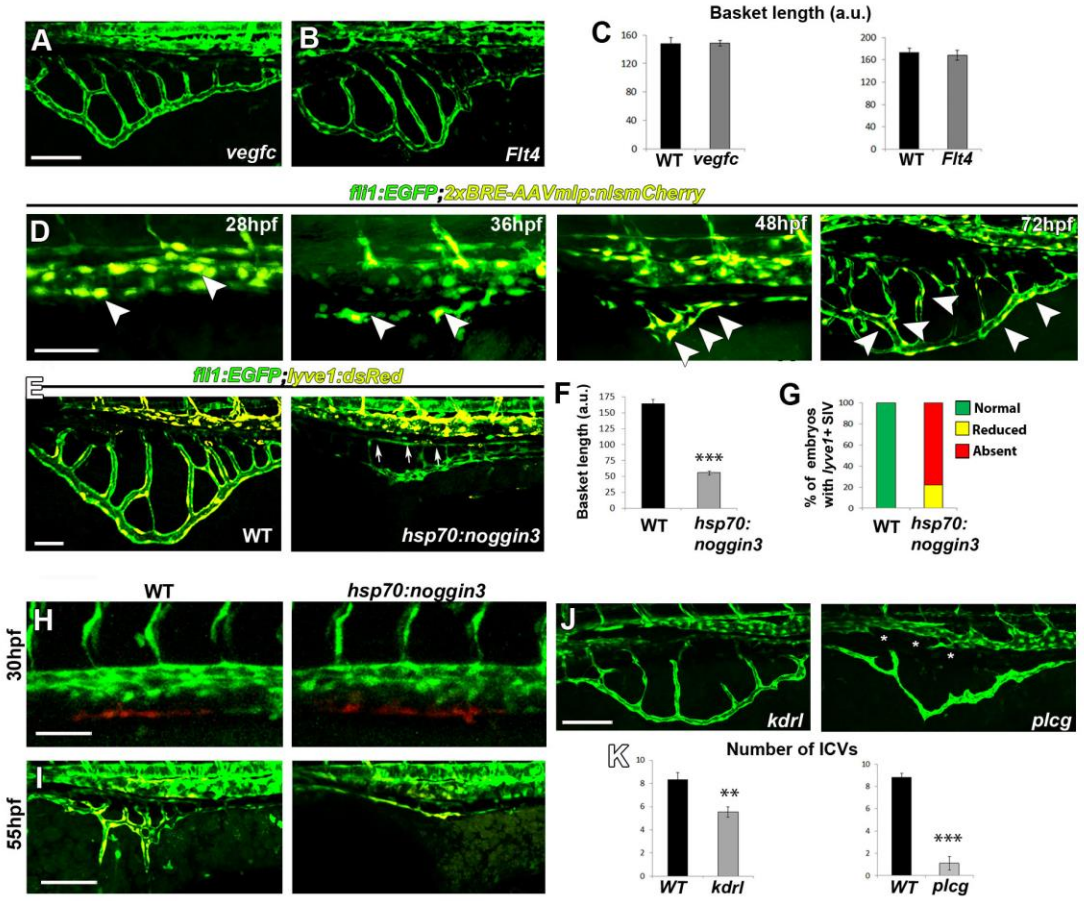

Figure 8. Molecular mechanisms controlling formation of the subintestinal plexus

Subintestinal vessels form normally in *vegfc* (**A,C**) and *flt4* (**B,C**) mutants. **D.** Activation of BMP signaling is detected in the PCV (28 hpf, arrowheads) and SIV (36-72 hph, arrowheads) of *Tg(2xBRE-AAVmlp:nlsmCherry)* embryos**. E-G.** Heat-shock induction of Noggin3 expression in *Tg(fli1:EGFP; lyve1:dsRed; hsp70l:noggin3)* embryos inhibits ventral migration of the plexus, as manifested by reduced basket length when compared to *Tg(fli1:EGFP; lyve1:dsRed*) (WT) embryos (**E,F**). The SIA forms normally (**E**, arrows). Cells in the SIV of *noggin3*-overexpressing embryos fail to upregulate the lymph-venous marker *lyve1* (**E,G**). **H,I**. The vPCV of *Tg(fli1:gal4;uas:kaede)* (WT) and *Tg(fli1:gal4;uas:kaede;hsp70l:noggin3)* double transgenic embryos was photoconverted at 30 hpf (**H**). At 55 hpf red labeled ECs were detected in the SIV of both WT and *hsp70l:noggin3* overexpressing embryos (**I**). **J,K.** Impaired Vegf signaling results in reduced number of ICVs in *kdrl* and *plcg* mutants (**J,K**). The SIA is absent in plcg mutants (**J**, asterisks). Scale bar: 50 µm.n_{VegfC}=19; n_{Flt4}=5; $n_{noggin3}$=11; n_{kdrl}=13; n_{plcg}=9. ***P*<0.01; ****P*<0.001.

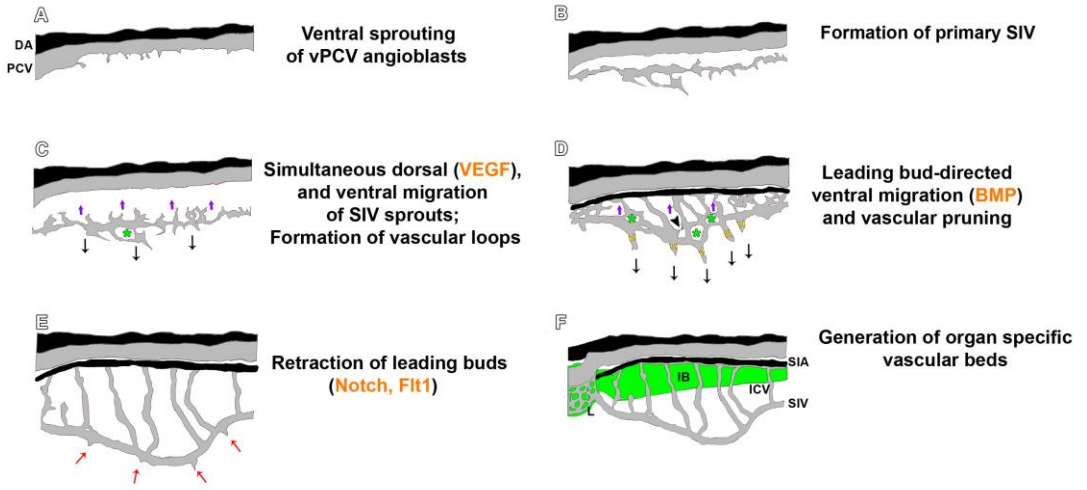

Figure 9. Molecular and cellular mechanisms underlying the formation of the GI vasculature

Schematic illustration depicting the different steps, and molecular cues involved in development of the subintestinal plexus. Black arrows- ventral sprouting and ventral migration, purple arrows- ECs "lagging-back" and dorsal migration, black arrowhead-vessel pruning, green asterisks- vascular loops. DA, dorsal aorta; IB, intestinal bulb; L, Liver; ICVs, inter-connecting vessels; PCV, posterior cardinal vein; SIA, supraintestinal artery; SIV, subintestinal vein**.**

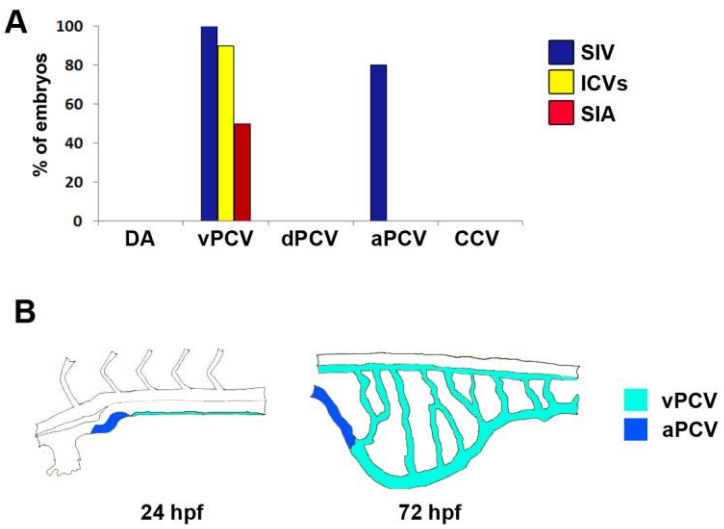

Figure S1. Fate map analysis of the subintestinal vessels

(A) Percentage of embryos with red-labeled ECs found in the SIV, ICVs and SIA at 3 dpf, following photoswitching of the indicated vessel (X axis) at 1 dpf. (B) Schematic diagram summarizing the origin of each vessel in the subintestinal plexus. aPCV, anterior PCV; CCV, common cardinal vein; DA, dorsal aorta; dPCV, dorsal PCV; vPCV, ventral PCV; SIV, subintestinal vein. n_{DA}=24, n_{CCV}=11, n_{vPCV}=16, n_{dPCV}=10, n_{aPCV}=5.

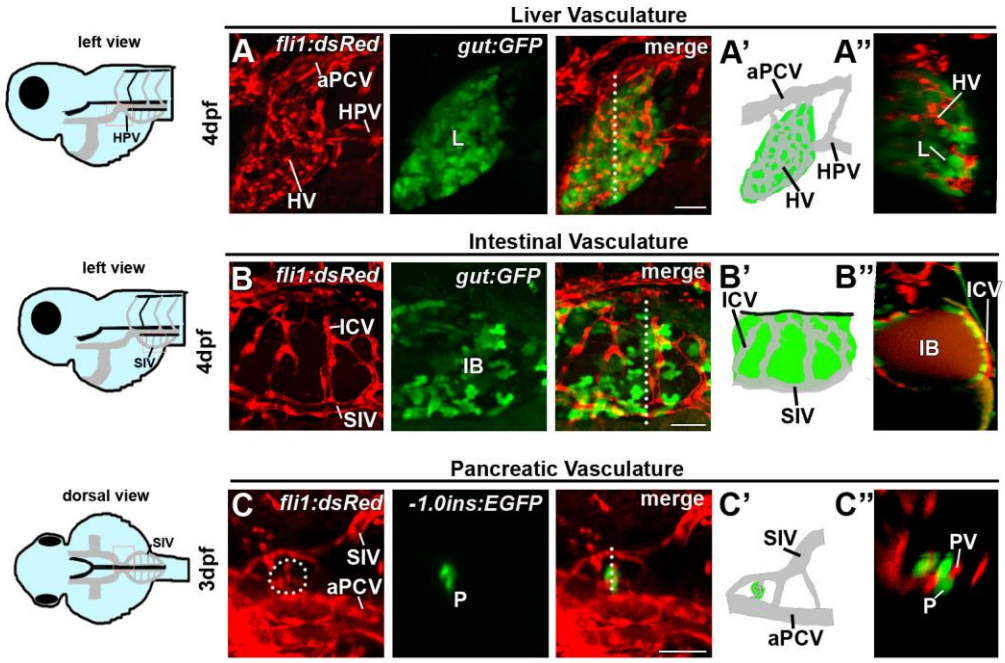

Figure S2: Anatomical distribution of the gastrointestinal organs and their vasculature

(A-C) Confocal images of *Tg(gut:GFP;fli1:dsRed)* (A,B) and *Tg(-1.0ins:EGFP; fli1:dsRed)* (C) embryos at 3-4 dpf. (A'-C') Explanatory diagrams of the corresponding confocal images, depicting the relative position of veins (grey), arteries (black), and organs (green). (A''-C'') Digital sections (10-15µm) performed at the approximate position indicated by the dashed line. (A-A'') Hepatic vessels (HV) surround and penetrate the liver (L) by 4 dpf, and connect to the hepatic portal vein (HPV) and aPCV. (B-B'') The SIV, SIA and ICVs vascularize the intestinal bulb (IB). (C-C'') The first right ICV interconnects the right SIV with the SIA, and gives rise to vessels penetrating the pancreatic anlage. aPCV, anterior PCV; HPV, hepatic portal vein; HV, hepatic vessels; ICV, interconnecting vessels; SIV, subintestinal vein; IB, intestinal bulb; P, pancreas; PV, pancreatic vessels. Scale bars: 50µm.

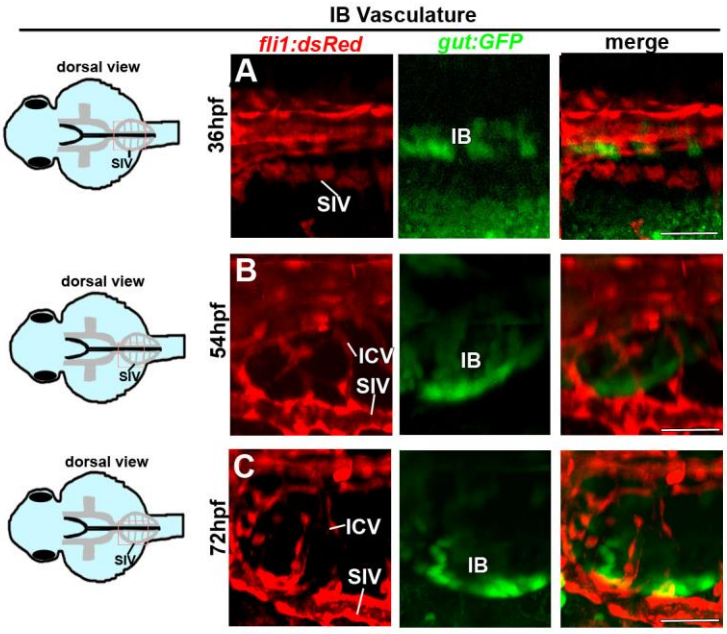

Figure S3: The intestinal bulb develops in close contact to the subintestinal vessels

(A-C) Confocal images of *Tg(gut:GFP;fli1:dsRed)* embryos at 36-72 hpf showing morphogenesis and growth of the intestinal bulb (IB) and its vasculature arising from the ICVs and SIV. ICV, interconnecting vessel; IB, intestinal bulb; SIV, subintestinal vein. Scale bars: 50µm.

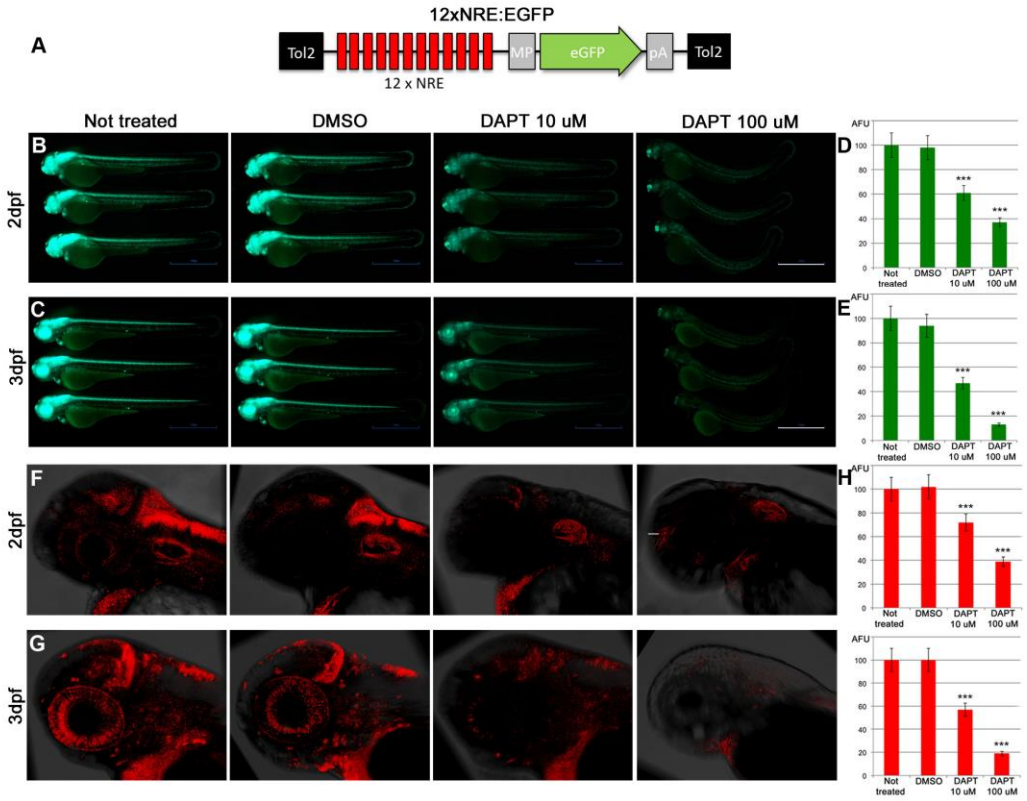

Figure S4. Generation and validation of a 12xNRE:EGFP Notch signaling reporter

(A) Schematic illustration of the 12xNRE Notch reporter, consisting of 12 Notch-responsive elements (12xNRE) and a rabbit β-globin minimal promoter (MP), followed by enhanced GFP (eGFP) and polyA (pA) tail, flanked by Tol2 elements. (B,C) Dose-response of Notch signaling in 12xNRE:EGFP embryos, following treatment with the Notch signaling inhibitor DAPT. (D,E) Quantification of EGFP intensity following treatments in B and C**.** Results are shown in arbitrary fluorescence units (AFU). *n*=6 per treatment. ****P*<0.0001. (F,G) Fluorescent *in situ* hybridization for EGFP following DMSO or DAPT treatment. (H,I) Quantification of fluorescence detected following treatments in F and G. *n*=6 for each treatment. ****P*<0.0001. Embryos were exposed to 10 or 100 µM DAPT, or DMSO, from 24 to 48 hpf (B,D) or from 24 to 72 hpf (C,E). Scale bars: 100µm.

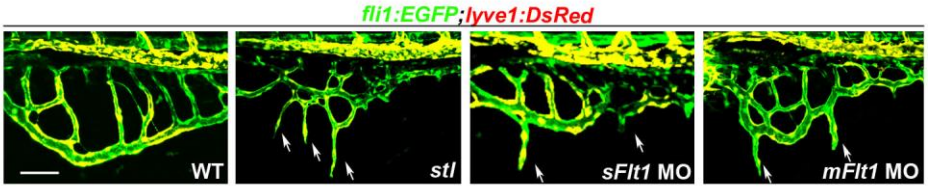

Figure S5. Impaired Notch and Flt1 signaling does not affect venous-fate of the SIV

Downregulation of *flt1* in *stl* mutants or *flt1* morphants resulted in *lyve1:dsRed*-positive (colocalization in yellow) ectopic leading buds along the SIV (arrows). Scale bars: 50 µm.

Supplemental Movies

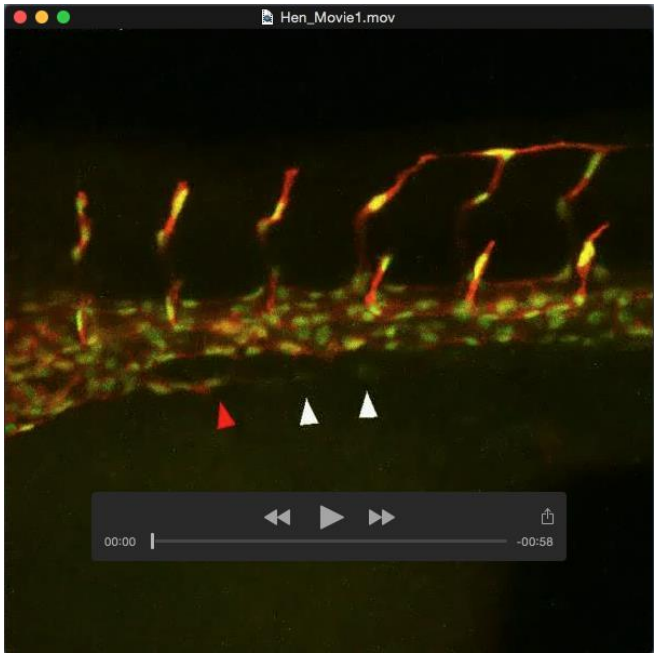

Movie 1: Different mechanisms of EC migration underlie the formation of the subintestinal plexus. This movie shows time-lapse images of the a *Tg(fli1: dsRed;fli1:nGFP)* zebrafish embryo between 32-90 hpf. Individual sprouts from the vPCV (white arrowheads) anastomose and fuse with a projection from the anterior PCV (red arrowhead), to generate a primary SIV. Sprouts elongating dorsally from the SIV generate the SIA (blue arrowheads). After collective ventral migration and retraction of the leading buds (arrows) the final shape of the basket is achieved.

Movie 2: aPCV and SIV vessels give rise to the pancreatic vasculature. This movie shows time-lapse images of photoswitched cells in the right aPCV and right SIV of a *Tg(fli1:gal4;uas:kaede;-1.0ins:EGFP*) zebrafish embryo between 54-73.5 hpf. Cells from the aPCV (arrowhead) and from the SIV (arrow) generate the pancreatic vasculature surrounding and penetrating the nascent pancreas (P, *insulin:EGFP*$^{+}$). The first frame was acquired immediately after photoswitching.

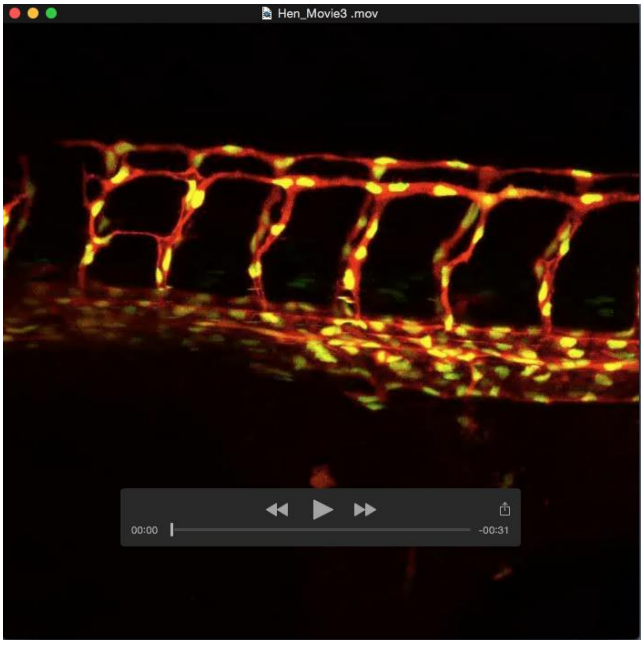

Movie 3: vPCV angioblasts give rise to all components of the subintestinal plexus. This movie shows time-lapse images of the a *Tg(fli1:dsRed;fli1:nGFP)* zebrafish embryo between 31.5-69.75 hpf. A selected vPCV angioblast was colored off-line in light-blue. vPCV angioblasts sprout ventrally incorporating into the primary SIV. Later on, they migrate dorsally to populate the SIA.

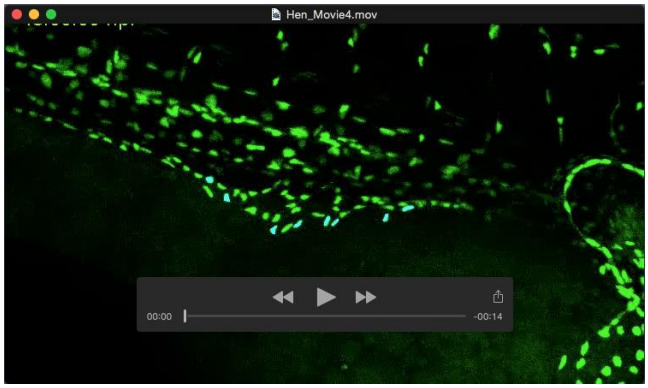

Movie 4: "Leading buds" guide the ventral migration of the subintestinal plexus. This movie shows time-lapse images of the a *Tg*(*fli1:nGFP)* zebrafish embryo between 48-69 hpf. Leading buds, consisting of paired ECs (colored off-line in light-blue) migrate ventrally. By the end of the remodeling phase, these sprouts retract and incorporate into the SIV.

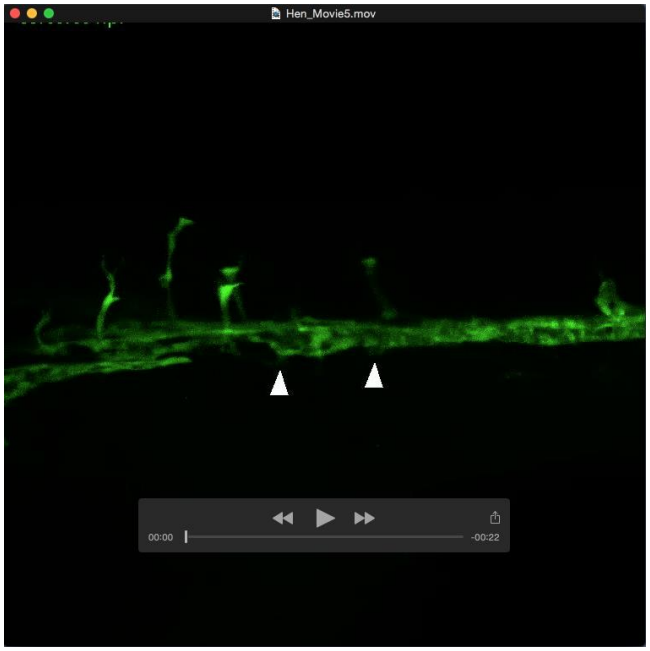

Movie 5: *kdrl* mutants exhibit defective dorsal migration and malformed ICVs. This movie shows time-lapse images of *kdrl* mutants on a *Tg*(*fli1:EGFP)* background, between 33 to ~60 hpf. While the formation of the SIV is normal (arrowhead), the subintestinal plexus shows a reduced number of ICVs (asterisks).

Movie 6: *plcg1* mutants exhibit defective dorsal migration and absent SIA. This movie shows time-lapse images of *plcg1* mutant on a *Tg(fli1:EGFP)* background, between 32-62 hpf. While the formation of the SIV is normal (arrowhead), no SIA is formed (asterisks).